ATTACHMENT 1

Palo Verde Nuclear Generating Station Unit 3 Reactor Coolant Pump 2A Suction Safe End Instrumentation Nozzle Half-Nozzle Repair Evaluation, WCAP-18051-NP, Non-proprietary Version

Notes:

- This Attachment provides a non-proprietary version of the document provided in Attachment 2 to this Enclosure.
- An affidavit is appended to the end of this Attachment and applies to the proprietary version of the document provided in Attachment 2. The affidavit provides the bases for withholding the proprietary document from public disclosure, pursuant to 10 CFR 2.390.
- The redactions noted in this Attachment are annotated to indicate the corresponding bases for withholding the information from public disclosure and correspond to the bases as enumerated in the appended affidavit.

WCAP-18051-NP
Revision 0

October 2015

Palo Verde Nuclear Generating Station Unit 3 Reactor Coolant Pump 2A Suction Safe End Instrumentation Nozzle Half-Nozzle Repair Evaluation

Westinghouse

WCAP-18051-NP
Revision 0

Palo Verde Nuclear Generating Station Unit 3 Reactor Coolant Pump 2A Suction Safe End Instrumentation Nozzle Half-Nozzle Repair Evaluation

Matthew T. Coble*
Major Reactors Components Design and Analysis – I

Nathan L. Glunt*
Piping Analysis and Fracture Mechanics

October 2015

Reviewer: James P. Burke*
Major Reactors Components Design and Analysis – I

Anees Udyawar*
Piping Analysis and Fracture Mechanics

Approved: Carl J. Gimbrone*, Manager
Major Reactors Components Design and Analysis - I

John L. McFadden*, Manager
Piping Analysis and Fracture Mechanics

*Electronically approved records are authenticated in the electronic document management system.

Westinghouse Electric Company LLC
1000 Westinghouse Drive
Cranberry Township, PA 16066, USA

© 2015 Westinghouse Electric Company LLC
All Rights Reserved

TABLE OF CONTENTS

LIST OF TABLES iv

LIST OF FIGURES v

1 BACKGROUND AND INTRODUCTION 1-1
2 FINITE ELEMENT MODELING 2-1
2.1 METHOD DISCUSSION 2-1
2.2 MESHED MODEL 2-1
2.3 FEM MATERIAL 2-4
2.4 THERMAL AND PRESSURE TRANSIENTS 2-4
2.5 BOUNDARY CONDITIONS 2-15
2.5.1 Thermal Boundary Conditions 2-15
2.5.2 Structural Boundary Conditions 2-15
2.5.3 Mechanical Loads 2-20
2.5.4 Instrumentation Nozzle Inertial Loads 2-22
2.6 STRESS PATH LOCATIONS 2-24
2.6.1 Fracture Mechanics Evaluation Paths 2-24
2.6.2 Section III Evaluation Paths 2-26
2.7 FINITE ELEMENT RESULTS FOR USE IN FRACTURE MECHANICS EVALUATIONS 2-30
3 ASME SECTION III EVALUATION 3-1
3.1 ACCEPTANCE CRITERIA 3-1
3.1.1 ASME Section III Design Rules 3-1
3.1.2 Section III Evaluation Stress Allowable Values 3-3
3.1.3 Design Fatigue Curves for Section III Analysis 3-8
3.2 STRESS RESULTS 3-10
3.2.1 Design Condition 3-10
3.2.2 Normal and Upset Conditions (Levels A and B) 3-11
3.2.3 Test Conditions 3-11
3.2.4 Faulted Condition (Level D) 3-12
3.2.5 Fatigue Evaluation 3-13
3.3 VIBRATION ASSESSMENT 3-13
4 FRACTURE MECHANICS EVALUATION 4-1
4.1 METHODOLOGY 4-1
4.1.1 Fatigue Crack Growth 4-2
4.1.2 Structural Integrity of the RCP Suction Safe End 4-3
4.1.3 Generation of Stress Intensity Factors 4-9
4.1.4 Transient Stress Analysis 4-12
4.1.5 Welding Residual Stress Analysis 4-13
4.2 FRACTURE MECHANICS EVALUATION RESULTS 4-20
4.2.1 Fatigue Crack Growth Evaluation 4-20
4.2.2 Final Flaw Stability Evaluation 4-21
4.2.3 Corrosion 4-33
4.3 FRACTURE MECHANICS SUMMARY AND CONCLUSIONS 4-34
5 LOOSE PARTS EVALUATION 5-1
6 SUMMARY AND CONCLUSION 6-1
7 REFERENCES 7-1

APPENDIX A : ASME STRESS PATH LOCATIONS A-1
A.1 RCP SUCTION NOZZLE SAFE END LIMITING PATHS A-1
A.2 REPLACEMENT NOZZLE LIMITING PATHS A-5
A.3 ATTACHMENT WELD LIMITING PATHS A-8

LIST OF TABLES

Table 2-1: Transients 2-4
Table 2-2: Mechanical Loads on Cold Leg Pipe from [26] 2-21
Table 2-3: NOp Loads without Deadweight 2-22
Table 2-4: Pressure Instrumentation Nozzle Mechanical Loads from [27] 2-22
Table 2-5: Response Spectra at [ ]^{a,c,e} Hz 2-22
Table 2-6: Instrumentation Nozzle Inertial Loads 2-23
Table 3-1: Material Strength Properties 3-4
Table 3-2: ASME Load Case Combinations 3-4
Table 3-3: Section III Allowable Stresses for RCP Suction Nozzle Safe end, 1974 Code Year [2] 3-6
Table 3-4: Section III Allowable Stresses for Replacement Nozzle and Weld, 1998 Code Year [3] 3-7
Table 3-5: Design Condition Stress Results 3-10
Table 3-6: Normal and Upset Condition Stress Results 3-11
Table 3-7: Test Condition Stress Results 3-11
Table 3-8: Faulted Condition Stress Results 3-12
Table 3-9: Fatigue Evaluation Results 3-13
Table 4-1: ASME Section XI, Appendix C Safety Factors 4-6
Table 4-2: Fatigue Crack Growth Results 4-21
Table 4-3: Screening Criteria Results for Limiting Transient Time Steps 4-22
Table 4-4: LEFM Results for Axial Flaw 4-24
Table 4-5: LEFM Results for Circumferential Flaw 4-24
Table 4-6: EPFM Results for Axial and Circumferential Flaws at 0.1" Crack Extension 4-26
Table 4-7: Palo Verde Unit 3 RCP Suction Safe End Primary Stress Limit 4-32

LIST OF FIGURES

Figure 1-1: RCP Instrumentation Nozzle Repair Schematic 1-3
Figure 2-1: FEM (Overall Section Cut through X-Y Plane) 2-2
Figure 2-2: FEM (Close-up View of Pressure Instrumentation Region) 2-3
Figure 2-3: Plant Heatup 2-5
Figure 2-4: Plant Cooldown 2-6
Figure 2-5: Plant Loading 2-7
Figure 2-6: Plant Unloading 2-8
Figure 2-7: Reactor Trip – Envelope of Reactor Trip, Loss of Flow, and Loss of Load 2-9
Figure 2-8: 10% Step Increase 2-10
Figure 2-9: 10% Step Decrease 2-11
Figure 2-10: Loss of Secondary Pressure (0 to 4,000 Seconds) 2-12
Figure 2-11: Loss of Secondary Pressure (Full Range) 2-13
Figure 2-12: Leak Test 2-14
Figure 2-13: RCS Temperature Surfaces 2-15
Figure 2-14: Fixed Boundary Conditions 2-17
Figure 2-15: Mechanical Load Boundary Conditions 2-18
Figure 2-16: Pressure Surfaces 2-19
Figure 2-17: Safe end Blowoff Pressure 2-19
Figure 2-18: Instrumentation Nozzle Blowoff Load 2-20
Figure 2-19: Flaw Evaluation Paths 2-24
Figure 2-20: Stress Orientation for Downstream Flaw Evaluation 2-25
Figure 2-21: Typical Paths in RCP Suction Nozzle Safe end 2-26
Figure 2-22: Typical Paths in Attachment Weld Cross-section 2-27
Figure 2-23: Typical Paths in Nozzle Body Cross-section 2-27
Figure 2-24: Typical Primary Membrane (P_m) Weld Path Locations 2-28
Figure 2-25: Typical Path Locations in Nozzle Fillet Region 2-29
Figure 2-26: Typical Path Locations in Outboard End Region of Nozzle 2-29
Figure 2-27: Stress Intensity Contour Plot, End of Cooldown 2-30
Figure 2-28: Stress Intensity Contour Plot, Reactor Trip at Time = 62.9 Seconds 2-31
Figure 2-29: Stress Intensity Contour Plot, Loss of Secondary Pressure at Time = 75 Seconds 2-32
Figure 3-1: Attachment Weld Design Requirements [3] 3-2
Figure 3-2: Socket Weld Design Criteria [28] 3-3
Figure 3-3: Design Fatigue Curve for SA-508 Class 1, per Figure I-9.1 [2] 3-8
Figure 3-4: Design Fatigue Curve for SB-166, per Figure I-9.2.1 and Figure I-9.2.2 [3] 3-9
Figure 4-1: Corner Crack Geometry 4-10
Figure 4-2: Axial Flaw Geometry 4-10
Figure 4-3: Circumferential Flaw Geometry 4-11
Figure 4-4: Residual Stress Evaluation Cut Paths [13] 4-15
Figure 4-5: Residual Hoop Stress Results (psi) [13] 4-16
Figure 4-6: Residual Axial Stress Results (psi) [13] 4-17
Figure 4-7: Through-Wall Welding Residual Hoop Stress Profile [13] 4-18
Figure 4-8: Through-Wall Welding Residual Axial Stress Profile [13] 4-19
Figure 4-9: EPFM Evaluation Results for Axial Flaw – Step Load Increase Transient 4-26
Figure 4-10: EPFM Evaluation Results for Axial Flaw - Reactor Trip Transient 4-27

Figure 4-11: EPFM Evaluation Results for Axial Flaw - Loss of Secondary Pressure Transient.....4-28
Figure 4-12: EPFM Evaluation Results for Circumferential Flaw - Step Load Increase Transient.....4-29
Figure 4-13: EPFM Evaluation Results for Circumferential Flaw - Reactor Trip Transient.....4-30
Figure 4-14: EPFM Evaluation Results for Circumferential Flaw - Loss of Secondary Pressure Transient.....4-31
Figure A-1: Path Location 6.....A-1
Figure A-2: Path Location 1.....A-2
Figure A-3: von Mises Stresses - Cooldown Transient at Step 5, Time 16,664 Seconds.....A-3
Figure A-4: von Mises Stresses - 10% Step Increase Transient at Step 4, Time 686 Seconds.....A-4
Figure A-5: Path Location 61.....A-5
Figure A-6: Path Locations 58 and 60.....A-6
Figure A-7: von Mises Stresses - Cooldown Transient at Step 4, Time 10,800 Seconds.....A-6
Figure A-8: von Mises Stresses - Upset Transient at Step 5, Time 62.89 Seconds.....A-7
Figure A-9: Path Location 26.....A-8
Figure A-10: Path Location 31.....A-9
Figure A-11: Path Location 39.....A-9
Figure A-12: Path Location 27.....A-10
Figure A-13: Path Location 19.....A-10
Figure A-14: Path Location 35.....A-11
Figure A-15: von Mises Stresses - Cooldown Transient at Step 5, Time 16,664 Seconds with Cutout at Path 39.....A-12
Figure A-16: von Mises Stresses - 10% Step Increase Transient at Step 4, Time 686 Seconds with Cutout at Path 39.....A-13

1 BACKGROUND AND INTRODUCTION

During the 3R18 spring 2015 refueling outage at Palo Verde Nuclear Generating Station (PVNGS) Unit 3, visual examinations of the reactor coolant pump (RCP) suction safe end revealed evidence of leakage in the annulus between the outer surface of the Alloy 600 instrument nozzle and the bore on the suction safe end. The most likely location of the flaw(s) is in the primary water stress corrosion cracking (PWSCC)-susceptible Alloy 82/182 weld and Alloy 600 instrument nozzle, along their fusion line inside the safe end bore. The Alloy 600 instrument nozzle is attached with a partial penetration weld to the inside of the RCP suction safe end.

The "half-nozzle" repair method was used to replace a portion of the Alloy 600 one-inch instrument nozzle as an alternative to the ASME Section XI [1] requirement to correct the observed leakage. The repair was made with an Alloy 690 PWSCC-resistant material half-nozzle, which was attached to the Palo Verde Unit 3 RCP suction safe end outside diameter. For the half-nozzle repair [5], the instrument nozzle is severed on the outside of the RCP suction safe end. The remaining lower portion of the instrument nozzle is removed by boring into the suction safe end. The removed portion of the Alloy 600 instrument nozzle is then replaced with a section (half-nozzle) of a more PWSCC-resistant Alloy 690 material, which will then be welded to the outside surface of the suction safe end using a 52M weld filler (see Figure 1-1). The inner portion of the original instrument nozzle, including the partial penetration weld, is left in place.

The half-nozzle repair has been successfully implemented on 73 Alloy 600 small-bore reactor coolant system hot leg nozzles (i.e., pressure taps, sampling line, and resistive temperature device thermowell nozzles) for Palo Verde Units 1, 2, and 3 [6, 7, 30, and 31]. Additionally, the half-nozzle method has been used at many other Combustion Engineering (CE) designed nuclear steam supply system plants.

The purpose of this report is to demonstrate the acceptability of the half-nozzle repair for the flawed RCP suction safe end instrument nozzle at Palo Verde Unit 3 based on the following assessments:

- ASME Section III, Class 1 design analysis and Code reconciliation, including an evaluation of the Class 2 socket weld between the instrument nozzle and piping
- Corrosion evaluation
- ASME Section XI fracture mechanics evaluation
- Stress corrosion cracking assessment
- Loose parts evaluation

A detailed ASME Section III, Class 1 design analysis (Section 3) is performed to design the replacement weld and associated new half-nozzle. The evaluations consider the primary stress, secondary stress, and fatigue usage factors in the existing suction nozzle safe end material, replacement nozzle and weld. The evaluations consider the change in the Class 1 pressure boundary due to moving the weld location and corrosion effects.

The fracture mechanics evaluation (Section 4) will demonstrate that any flaws in the partial penetration J-groove weld that remain after the half-nozzle repair will not grow to an unacceptable flaw size into the suction safe end carbon steel metal for the remaining life of the plant.

A loose parts evaluation (Section 5) is performed to evaluate the effect that a postulated loose weld fragment(s) of the instrument nozzle partial penetration weld might have on a reactor coolant system (RCS) structure, system, or component (SSC).

Portions of this report contain proprietary information. Proprietary information is identified and bracketed. For each of the bracketed sections, the reasons for the proprietary classification are provided using superscripted letters "a", "c", and "e". These letter designations are:

a. The information reveals the distinguishing aspects of a process or component, structure, tool, method, etc. The prevention of its use by Westinghouse's competitors, without license from Westinghouse, gives Westinghouse a competitive economic advantage.

c. The information, if used by a competitor, would reduce the competitor's expenditure of resources or improve the competitor's advantage in the design, manufacture, shipment, installation, assurance of quality, or licensing of a similar product.

e. The information reveals aspects of past, present, or future Westinghouse- or customer-funded development plans and programs of potential commercial value to Westinghouse.

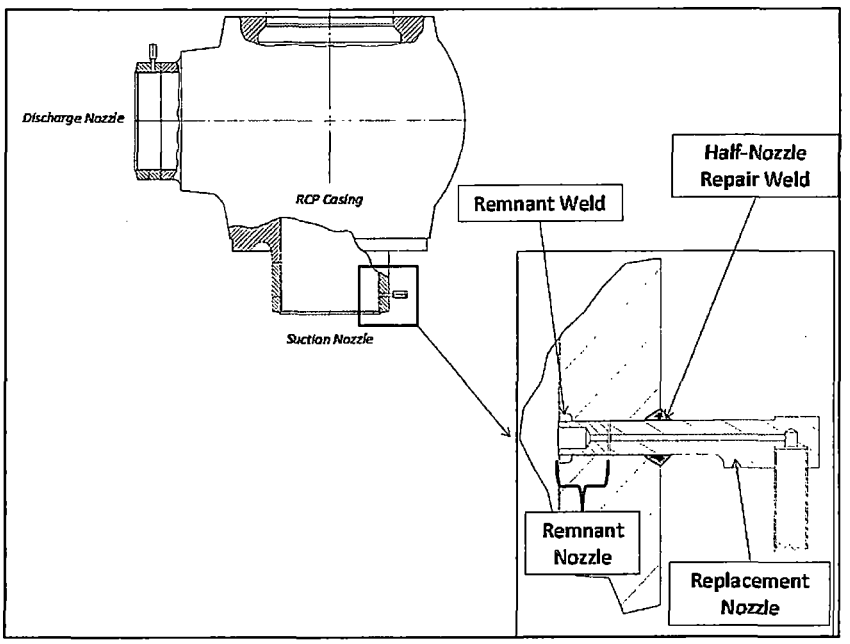

Figure 1-1: RCP Instrumentation Nozzle Repair Schematic

2 FINITE ELEMENT MODELING

A three-dimensional finite element model (FEM) of the RCP suction nozzle safe end, the remnant nozzle, remnant weld, half-nozzle replacement nozzle, and the half-nozzle repair weld was created. This model was used to perform an ASME Section III analysis and was used to determine the through-wall time history stresses for a fracture mechanics evaluation.

2.1 METHOD DISCUSSION

An ANSYS®[1] [18] FEM is created using the RCP and half-nozzle repair drawings [19]. The FEM is a three-dimensional model that includes the RCP suction nozzle safe end, the remnant nozzle, remnant nozzle-to-safe end internal J-groove weld, replacement nozzle, and external J-groove weld to the safe end outer diameter. A temperature degree of freedom (DOF) model and a displacement DOF model are created. The temperature DOF model will input thermal transients and will generate time-varying temperature profiles. The temperature profiles, system pressure transients, RCP nozzle safe end mechanical loads, and pressure instrumentation nozzle mechanical loads are input to the displacement DOF model, resulting in output time-varying stress profiles. Static runs containing uniform temperature, pressure, and mechanical loads are performed for seismic, accident, and design conditions. Stresses and temperatures through paths through the pipe base metal, pressure tap nozzle weld, and cladding will be output for downstream flaw evaluations. An ASME Section III evaluation is performed on the transient and static cases.

2.2 MESHED MODEL

The pressure measurement instrument half-nozzle repair and RCP suction nozzle safe end FEM is shown in Figure 2-1. A three-dimensional model is developed in ANSYS [18] with SOLID70, SOLID87, and SOLID90 elements for the temperature DOF model, and with SOLID185, SOLID186, and SOLID187 elements for the displacement DOF model. An overall view of the FEM and a view of the region of interest are shown in Figure 2-1 and Figure 2-2, respectively. The FEA analysis included an inside diameter bore of [ ]^{a,c,e} inches which is equivalent to a diametric corrosion of [ ]^{a,c,e} inch. This is greater than the allowable of [ ]^{a,c,e} inch and also greater than the projected corrosion value of 0.1224 inch in 40 years, thus it is conservative. For the temperature DOF model, water mesh is included in the instrumentation region between the remnant nozzle, the safe end, and the replacement nozzle, up to the Class 1 pressure boundary at the instrumentation nozzle to piping weld. The water mesh is removed from the displacement DOF model for the stress runs because it does not carry load or contribute to stiffness.

The safe end portion of the model was extended 40 inches beyond the bottom safe end boundary to offset the mechanical load application point. The load application point requires rigid beams which locally

[1] ANSYS, ANSYS Workbench, Ansoft, AUTODYN, CFX, EKM, Engineering Knowledge Manager, FLUENT, HFSS and any and all ANSYS, Inc. brand, product, service and feature names, logos and slogans are trademarks or registered trademarks of ANSYS, Inc. or its subsidiaries located in the United States or other countries. ICEM CFD is a trademark used by ANSYS, Inc. under license. CFX is a trademark of Sony Corporation in Japan. All other brand, product, service and feature names or trademarks are the property of their respective owners.

over-restrains the model for radial growth due to pressure. The offset distance isolates the region of interest from the stresses associated with this load application method. The extra distance requires the input moments to be adjusted to remove the extra moment produced by the lateral (i.e., x-direction and z-direction) forces applied at the 40 inch moment arm. The moment adjustments are:

$$M_{x,adjusted} = M_{x,applied} + F_{z,applied} \times r \qquad \text{Equation 2-1}$$

$$M_{z,adjusted} = M_{z,applied} - F_{x,applied} \times r \qquad \text{Equation 2-2}$$

In Equation 2-1 and Equation 2-2 above, r is the 40 inch model extension, and $F_{applied}$ and $M_{applied}$ are the input loads applied to the suction nozzle safe end.

a,c,e

Figure 2-1: FEM (Overall Section Cut through X-Y Plane)

a,c,e

Figure 2-2: FEM (Close-up View of Pressure Instrumentation Region)

2.3 FEM MATERIAL

The material properties used in the analysis are from the 1974 ASME Code, Section II, Subsection NA without addenda [2] for the original geometry, and from the 1998 ASME Code, Section II, Part D [3] for the replacement pressure instrumentation nozzle and repair weld. The displacement DOF model inputs are elastic modulus, Poisson's ratio, and the coefficient of thermal expansion. The temperature DOF model inputs are density, thermal conductivity, and specific heat. Poisson's ratio and density are not provided in [2] or [3], and are taken from Table PRD of the 2013 ASME Code, Section II Part D [4].

The cladding is SA-240 Type 304 [19(b)], the suction nozzle safe end is SA-508 Class 1 [20], the remnant pressure instrumentation nozzle is SB-166 Alloy 600 [21], and the replacement pressure instrumentation nozzle is SB-166 Alloy N06690 [19(e)]. The remnant weld and repair weld match the attached nozzle material properties (i.e., Alloy 600 for the remnant and Alloy 690 for the replacement nozzle). The thermal properties of water are obtained as a function of temperature at normal operation pressure of [ ]^{a,c,e} psia from [22].

2.4 THERMAL AND PRESSURE TRANSIENTS

The thermal and pressure transients for normal, upset, faulted, and test conditions used in this analysis are based on [22 and 23]. The transients are listed in Table 2-1 and are shown in Figure 2-3 through Figure 2-12. Hydrostatic Test is included for fracture mechanics evaluations. The design specification [22] specifies a maximum pressure of [ ]^{a,c,e} psia; however, Article IWB-5000 of [1] specifies a maximum value 1.1 times the operating pressure, or [ ]^{a,c,e} psia. For the analysis, a bounding value of [ ]^{a,c,e} psia was used. Reference [22] does not specify a temperature curve; therefore, it was assumed that the temperature transient matches the Leak Test temperature transient.

Table 2-1: Transients a,c,e

[ ]

a,c,e

Figure 2-3: Plant Heatup

a,c,e

Figure 2-4: Plant Cooldown

a,c,e

Figure 2-5: Plant Loading

a,c,e

Figure 2-6: Plant Unloading

a,c,e

Figure 2-7: Reactor Trip – Envelope of Reactor Trip, Loss of Flow, and Loss of Load

a,c,e

Figure 2-8: 10% Step Increase

a,c,e

Figure 2-9: 10% Step Decrease

a,c,e

Figure 2-10: Loss of Secondary Pressure (0 to 4,000 Seconds)

a,c,e

Figure 2-11: Loss of Secondary Pressure (Full Range)

a,c,e

Figure 2-12: Leak Test

Note: The leak test temperature transient is used to evaluate the hydrostatic test transient. The maximum pressure considered for hydrostatic test is [ ]^{a,c,e} psi.

2.5 BOUNDARY CONDITIONS

2.5.1 Thermal Boundary Conditions

The zone for temperature application is shown in Figure 2-13. The wetted zone for temperature includes just the inside cavity of the nozzle; further into the nozzle solid elements representing water mesh are included. The water acts only as a conductive heat transfer path and as thermal inertia; no natural convection is considered in this region. This is appropriate for stagnant water. The RCS flow rate is very large; therefore, it is appropriate to treat the heat transfer coefficient as infinite and directly apply the RCS temperature to the metal surface with the displacement constraint command (i.e., the metal surface temperature is instantaneously equal to the RCS water temperature). The pipe external surfaces are adiabatic because they are insulated. The sliced surfaces at the top and bottom of the safe end are adiabatic because the un-modeled structure would not significantly impact the thermal gradients in the region of interest. The temperature gradients would be radial, which is captured accurately with the adiabatic boundary condition.

a,c,e

Figure 2-13: RCS Temperature Surfaces

2.5.2 Structural Boundary Conditions

The fixed boundary conditions are shown in Figure 2-14. The top face of the cold leg nozzle safe end is restrained in the axial and circumferential directions. This provides sufficient fixity to prevent rigid body motion and to properly react out applied mechanical loads without over-restraining the model for radial thermal growth.

An array of rigid BEAM188 elements is located at the center of each load application region. These boundary conditions are shown in Figure 2-15. These elements are used to input the mechanical loads

from the RCS piping and instrument Class 2 piping to the FEM. The SOLID18X type elements do not have rotational degrees of freedom; therefore, the rigid BEAM188 elements transmit moments over a grouping of nodes on the solid elements.

The zone for pressure application is shown in Figure 2-16. Water is removed from the displacement DOF model and RCS pressure is applied on the entire inside surface of the pipe safe end and the pressure instrumentation nozzle. The pipe safe end is not capped; therefore, a blowoff pressure is calculated to generate the appropriate tensile load in the safe end. The blowoff pressure is based on the ratio of the uncapped open area to the cross-section area:

$$P_B = P\frac{{r_i}^2}{({r_o}^2 - {r_i}^2)} \qquad \text{Equation 2-3}$$

In Equation 2-3:

P_B = calculated blowoff pressure

P = applied RCS pressure

r_o = outer radius of annular cross-section

r_i = inner radius of annular cross-section

The inner radius used in the calculation of the safe end blowoff pressure includes the cladding, which is part of the FEM. The safe end blowoff pressure condition is shown in Figure 2-17.

The pressure instrumentation nozzle is also not capped, which results in an internal load acting in the +y direction. A blowoff load is applied to offset this internal load so that the forces balance in equilibrium. The load is equal to the internal pressure times the open area and acts in the -y direction. The load is applied to the same mass element used for the mechanical load application. The pressure instrumentation nozzle blowoff pressure condition is shown in Figure 2-18.

a,c,e

Figure 2-14: Fixed Boundary Conditions

a,c,e

Figure 2-15: Mechanical Load Boundary Conditions

a,c,e

Figure 2-16: Pressure Surfaces

a,c,e

Figure 2-17: Safe end Blowoff Pressure

a,c,e

Figure 2-18: Instrumentation Nozzle Blowoff Load

2.5.3 Mechanical Loads

RCP suction nozzle safe end loads are from [26]. The loads are provided for deadweight, five normal operation (NOp) cases, seismic condition, and accident conditions; see Table 2-2. The accident condition is the square root sum of the squares of SSE and rupture. The loads are provided in the global Cartesian coordinate system (where the x-axis is from the reactor to steam generator 2, the y-axis is vertical, and the z-axis follows with the right-hand rule). The suction nozzle is oriented in the vertical direction; therefore, the x-direction and z-direction loads are shear forces and bending moments, and the y-direction loads are axial force and torque.

The safe end NOp loads include deadweight. For this analysis, the time-varying portion of the NOp loads must be isolated so it can be scaled independently of deadweight. The deadweight load is subtracted from each of the five NOp load cases. Reference [26] indicates that the five NOp conditions are:

(1) deadweight + thermal without friction at full power

(2) deadweight with friction at start of heatup (70°F)

(3) deadweight + thermal with friction at end of heatup (565°F [22])

(4) deadweight + thermal with friction at start of cooldown (565°F from [22])

(5) deadweight with friction at end of cooldown (70°F)

These cases correspond directly to Heatup and Cooldown transients, and are applied coinciding with the temperature changes during the transients. For the Leak Test transient, the loads were interpolated for conditions (2) and (3) at 100°F and 400°F, respectively, as shown below:

$$f_{100°F} = F_2 + \frac{F_3 - F_2}{565°F - 70°F}(100°F - 70°F) \qquad \textbf{Equation 2-4}$$

$$f_{400°F} = F_2 + \frac{F_3 - F_2}{565°F - 70°F}(400°F - 70°F) \qquad \textbf{Equation 2-5}$$

In Equation 2-4 and Equation 2-5, F_2 and F_3 are the heatup loads corresponding to NOp conditions (2) and (3). The NOp minus deadweight loads are listed in Table 2-3. The loads are converted into lb_f and $in \cdot lb_f$ for the ANSYS FEM.

Pressure instrumentation nozzle mechanical loads from [27] are listed in Table 2-4. These loads are due to weight and inertial effects of the Class 2 piping on the nozzle. Inertia loads due to OBE, SSE, and branch line pipe break (BLPB) on the instrumentation nozzle itself will be derived in subsection 2.5.4.

Table 2-2: Mechanical Loads on Cold Leg Pipe from [26]

a,c,e

Notes:

(1) Seismic and accident loads are the square root of the sum of squares of the pipe load.
(2) accident = square root of the sum of squares (SSE, rupture)

Table 2-3: NOp Loads without Deadweight

[ ] a,c,e

Note:
(1) Maximum extreme values (positive or negative) are used for the NOp condition.

Table 2-4: Pressure Instrumentation Nozzle Mechanical Loads from [27]

[ ] a,c,e

Note:
(1) SSE loads can be positive or negative.

2.5.4 Instrumentation Nozzle Inertial Loads

The pressure instrumentation nozzle inertia loads are calculated by determining the lowest cantilever mode frequency of the nozzle and reading acceleration responses from various spectra plots at this frequency. A modal analysis of the Class 2 piping and a representation of the instrumentation nozzle provide a cantilever mode frequency of [ ]^{a,c,e} Hz. The design response spectra accelerations for seismic and BLPB loading for the instrument nozzle are listed in Table 2-5. The seismic spectra accelerations are 1% damping for OBE and 2% damping for SSE and BLPB. The nozzle mass is [ ]^{a,c,e} lbs. The inertial loads are equal to the spectra acceleration multiplied by the nozzle mass, and are listed in Table 2-6.

Table 2-5: Response Spectra at [ ]^{a,c,e} Hz

[ ] a,c,e

Table 2-6: Instrumentation Nozzle Inertial Loads a,c,e

2.6 STRESS PATH LOCATIONS

2.6.1 Fracture Mechanics Evaluation Paths

Paths are defined in ANSYS to generate temperature and stress profiles along a given path. The paths are shown in Figure 2-19. Paths 1 through 6 are located on the vertical plane intersecting the pressure instrumentation nozzle centerline and the safe end centerline (i.e., direction of hoop stress). Paths 7 through 12 are located on the horizontal plane intersecting the pressure instrumentation nozzle centerline. Paths 13 through 24 are not shown in the figure below for clarity, but are symmetric with respect to the paths 1 through 12 (i.e., paths 13 through 18 lie on the vertical plane below the instrumentation nozzle and paths 19 through 24 lie on the horizontal plane on the opposite side relative to paths 7 through 12). Stresses are provided in a cylindrical coordinate system where the x-direction is radial, the y-direction is circumferential, and the z-direction is axial. The cut paths are locally straight; therefore, the x-direction stress is a radial stress, the y-direction stress is a hoop stress, and the z-direction stress is an axial stress, as shown in Figure 2-20.

a,c,e

Figure 2-19: Flaw Evaluation Paths

a,c,e

Figure 2-20: Stress Orientation for Downstream Flaw Evaluation

2.6.2 Section III Evaluation Paths

The ASME evaluation is focused on stresses in the replacement pressure instrumentation nozzle, the weld between the replacement nozzle and the safe end, and region on the safe end around the instrumentation nozzle opening. Figure 2-21 through Figure 2-26 show typical paths used in the ASME evaluation. The term "cut" is used in the figures to denote a stress evaluation path. In general, all paths are repeated around the instrumentation nozzle in 90° intervals. Additional paths are also included to capture specific nodes with high stress ranges, not shown in the following figures.

Figure 2-21 shows the typical paths in the RCP suction nozzle safe end. These paths are shown with half of the nozzle opening hidden. There are twelve paths on the inner radius of the nozzle hole opening (in 30° intervals), and five paths on the outer radius of the hole opening near the chamfer cut for the remnant weld (paths 6 and 9 shown below). The paths on the inner radius of the nozzle hole opening are excluded from the primary membrane (P_m) stress check of the safe end because they are located at a peak stress location. Paths 6 through 9 are used for the P_m check on the safe end.

a,c,e

Figure 2-21: Typical Paths in RCP Suction Nozzle Safe end

Figure 2-22 shows the typical paths on the replacement nozzle weld. These paths are repeated in 90° intervals around the nozzle axis. Corresponding paths are set radially into the nozzle body at approximately equal nodes, as shown in Figure 2-23.

a,c,e

Figure 2-22: Typical Paths in Attachment Weld Cross-section

a,c,e

Figure 2-23: Typical Paths in Nozzle Body Cross-section

The paths in the weld region are divided, such that only paths on the primary shear plane of the weld are used in the primary membrane stress check. All other weld path membrane stresses are at peak stress locations. Paths 18, 19, 22, 23, 26, 27, 30, and 31 are included in the primary membrane (P_m) stress check. A cutaway of the weld is shown in Figure 2-24, with paths 18, 19, 30, and 31 shown.

a,c,e

Figure 2-24: Typical Primary Membrane (P_m) Weld Path Locations

Figure 2-25 and Figure 2-26 show the typical paths in the outer region of the replacement nozzle. These paths capture high stress areas in the fillet and transition region of the nozzle.

a,c,e

Figure 2-25: Typical Path Locations in Nozzle Fillet Region

a,c,e

Figure 2-26: Typical Path Locations in Outboard End Region of Nozzle

2.7 FINITE ELEMENT RESULTS FOR USE IN FRACTURE MECHANICS EVALUATIONS

Figure 2-27 through Figure 2-29 show the stress intensity contour plots for some of the limiting transient cases for the Cooldown, Reactor Trip, and Loss of Secondary Pressure that are evaluated in the fracture mechanics analysis.

a,c,e

Figure 2-27: Stress Intensity Contour Plot, End of Cooldown

Note: Stress displayed in the above figure is in units of psi.

a,c,e

Figure 2-28: Stress Intensity Contour Plot, Reactor Trip at Time = 62.9 Seconds

Note: Stress displayed in the above figure is in units of psi.

a,c,e

Figure 2-29: Stress Intensity Contour Plot, Loss of Secondary Pressure at Time = 75 Seconds

Note: Stress displayed in the above figure is in units of psi.

3 ASME SECTION III EVALUATION

An ASME Section III evaluation is performed to demonstrate the structural integrity of the half-nozzle repair geometry with regards to primary stresses, primary plus secondary stresses, and fatigue usage factors. Stress intensity values are calculated using the FEM detailed in Section 2. Primary, primary plus secondary, and peak stresses are evaluated using the paths shown in subsection 2.6.2.

3.1 ACCEPTANCE CRITERIA

Per the ASME Code reconciliation in [17], the replacement nozzle was procured to the 1998 ASME Code year up to and including 2000 Addenda [3]. The construction Code for the existing RCP is 1974 with no addenda [2]. Therefore, the existing material is qualified per the construction code [2], and the new replacement nozzle and attachment weld are qualified to the newer code year, 1998 with 2000 Addenda [3].

3.1.1 ASME Section III Design Rules

The welds connected to the new nozzle in this half-nozzle repair are governed by design rules in Section III of [2 and 3]. This includes the attachment weld connecting the replacement nozzle to the RCP safe end and the socket weld connecting the replacement nozzle to downstream Class 2 piping.

Attachment Weld

Per Section NB-3351.4 of [3], this is a Category D weld meeting the requirements of Section NB-4244(d) [3] for attachment of nozzles using partial penetration welds. Therefore, Figure NB-4244(d)-1 applies to this type of attachment weld. Section (c) of Figure NB-4244(d)-1 is the most applicable to this design, as shown here in Figure 3-1.

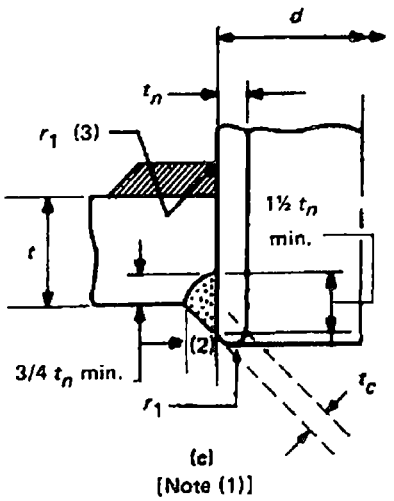

GENERAL NOTES:
(a) *Weld deposit reinforcement, if used, shall be examined as required in NB-5244.*
(b) The ¾ t_n min. dimension applies to the fillet leg and the J-groove depth.
(c) Weld groove design for oblique nozzles of this type requires special consideration to achieve the 1.25t_n minimum depth of weld and adequate access for welding inspection. With due regard to the requirements in Fig. NB-4244(c)-1, the welds shown in the sketches may be on either the inside or the outside. Weld preparation may be J-groove as shown or straight bevel. If weld deposit reinforcement is not used, *r*, shall apply to I.D. of base material instead of I.D. of weld buildup.
(d) For definitions of symbols, see NB-3352.4(d) for vessels and NB-3643 for piping.

FIG. NB-4244(d)-1 PARTIAL PENETRATION NOZZLE AND BRANCH PIPING CONNECTIONS

Figure 3-1: Attachment Weld Design Requirements [3]

The requirement for the size of the weld is that the groove depth be at least $3/4t_n$, where t_n is the nozzle body thickness. The nozzle body thickness, t_n, is equal to [ ]^{a,c,e} inches. The minimum required depth is 3/4 x [ ]^{a,c,e} inches = [ ]^{a,c,e} inches. The design weld depth is 1/2 inch, and is greater than the required [ ]^{a,c,e} inches. The $3/4t_n$ requirement also applies to the width of the fillet weld leg, as shown Figure 3-1. The fillet weld length is [ ]^{a,c,e} inches. This also meets the $3/4t_n$ requirement.

Figure NB-4244(d)-1, (c) of [3] also requires that the total weld size of the groove depth plus fillet leg height be a minimum of $1.5t_n$. The full weld size is 3/4 inches, which is greater than the required [ ]^{a,c,e} inches (1.5 x [ ]^{a,c,e} inches = [ ]^{a,c,e} inches).

Socket Weld

The Class 2 socket weld connecting the instrumentation nozzle to the downstream piping is qualified by designing the socket weld according to Section NC-3661.2 of [2]. Because the weld is sized according to design-by rules, it is qualified within the qualification of the existing Class 2 piping.

Section NC-3661.2 of [2] references Figure NC-4427-1, which calls for a fillet weld leg size of 1.09 times the piping thickness. The socket weld is designed in accordance with [28] using a 2:1 ratio. Using this 2:1 ratio, the minimum fillet weld leg is 1.09 times the piping thickness on the shorter leg and 2.18 times the thickness along the pipe axis. This layout is shown in Figure 3-2.

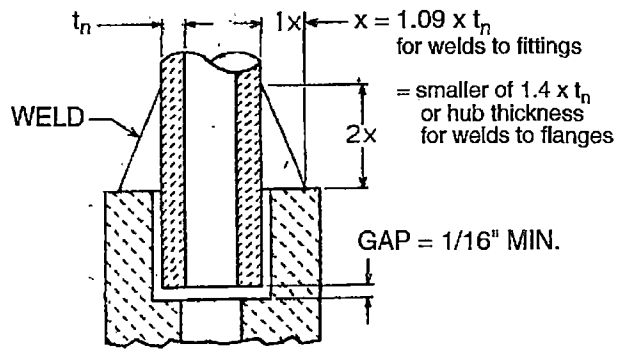

Figure 3-2: Socket Weld Design Criteria [28]

The attached Class 2 piping is 3/4-inch Schedule 160. The thickness of the pipe is [ ]^{a,c,e} inches. The minimum fillet leg sizes are [ ]^{a,c,e} inches and [ ]^{a,c,e} inches (1.09 x [ ]^{a,c,e} in = [ ]^{a,c,e} in, 2 x [ ]^{a,c,e} in = [ ]^{a,c,e} in). The socket weld fillet sizes of [ ]^{a,c,e} inches and [ ]^{a,c,e} inches exceed this requirement.

Section NC-3661.2 of [2] cites the ANSI Standard B16.11 [29]. However, the dimensional information in B16.11 is not a requirement, as discussed in Section 1.2 of [29]. All dimensions related to the design of the fitting (bore depth, diameter, etc.) have been designed on the replacement instrumentation nozzle to match the original design.

3.1.2 Section III Evaluation Stress Allowable Values

All stress evaluations are performed in accordance with Section NB-3200 of [2 and 3]. According to NB-3225, the rules of Appendix F of [2 and 3] apply for faulted conditions (service Level D). All stress intensities (SI) are derived in accordance with Section NB-3215 [2 and 3]. Stress intensity limits are in accordance with Figure NB-3221-1 for design conditions and Figure NB-3222-1 for normal and upset conditions (service Levels A and B). There are no emergency (Level C) conditions specified. Test conditions are evaluated in accordance with Section NB-3226. Special stress limits are evaluated for pure shear on the attachment weld for all loading conditions.

The pure shear check applies only to the weld paths. However, these checks are included for all paths for simplicity in post-processing.

Maximum Average Shear

Definition: $\tau_{max} = {}^{SI}/_{2}$

Maximum shear is set as half of the overall stress intensity for membrane stresses only. Membrane stresses are used because this is a stress check for pure shear, without consideration of bending. Therefore, $\tau_{max} = P_m/2$. This is the maximum overall shear stress for pure shear loading.

Table 3-1 lists the applicable S_m and S_y values for the RCP suction nozzle safe end and replacement instrumentation nozzle. The material strength properties for the replacement nozzle are used for evaluation of the attachment weld. The weld material used for this repair was ERNiCrFe-7A. This is a new weld material that did not exist in the 1974 or 1998/2000 ASME Codes. Therefore, the material properties for the weld filler material are taken from a recent version of ASME for comparison [4].

Section SFA-5.14/SFA-5.14M of Section II, Part C of [4] shows a minimum tensile strength for ERNiCrFe-7A filler metal of 85 ksi. This is slightly higher than the ultimate strength of the Alloy 690 base metal (S_u = 80 ksi, as shown in Table 3-1). Therefore, it is acceptable to use the material strength properties of the SB-166 alloy for the ERNiCrFe-7A weld filler material.

Table 3-1: Material Strength Properties

Component	Material	Material Reference	S_m (at 650°F)	S_y (at 400°F)(1)	S_u (at 650°F)	ASME Code Year
RCP Suction Nozzle Safe end	SA-508 Class 1 (Carbon Steel)	[20]	17.0 ksi	30.0 ksi	Note 2	1974 [2]
Replacement Instrumentation Nozzle	SB-166 Alloy N06690	[19(e)]	23.3 ksi	28.6 ksi	80.0 ksi	1998 [3]

Notes:

(1) The value of S_y is only used for the test condition allowable. Therefore, it is taken at the test condition temperature of 400°F.

(2) Values for ultimate strength, S_u, are not available in the 1974 Code year [2]. The ultimate strength is only used for the allowable stress under faulted conditions (minimum of $2.4S_m$ and $0.7S_u$). Therefore, the value of $2.4S_m$ is used for that allowable stress check.

Table 3-2 summarizes the load case combinations used for each load case as they apply to the ASME groupings of design, Levels A and B, Level D, and test conditions. There are no Level C conditions for this analysis.

Table 3-2: ASME Load Case Combinations

Condition	Case	Definition
Design	Design Conditions	Pressure + Deadweight Loads
Normal (Level A)	Plant Heatup	Applicable Pressure and Thermal Transient + Normal Operation Mechanical Loads
	Plant Cooldown	
	Plant Loading	
	Plant Unloading	
	10% Step Increase (+20°F, +100 psi)	
	10% Step Decrease (-20°F, -100 psi)	
Upset (Level B)	Reactor Trip, Loss of Flow, Loss of Load	Upset Pressure and Thermal Transient + Mechanical Load
	OBE	Normal Operation Pressure and Temperature ± Safe end and Instrumentation Nozzle OBE loads
Faulted (Level D)	Loss of Secondary Pressure	Loss of Secondary Pressure Thermal and Pressure Transient
	Safe Shutdown Earthquake (SSE)	Normal Operation Pressure and Temperature ± Accident Load
	SSE and Pipe Break	
Test	Leak Test	Leak Test Pressure and Thermal Transient + Normal Operation Mechanical Loads

Table 3-3 summarizes the allowable stresses for all loading conditions for the 1974 Code year [2], which is applicable to the SA-508 Class 1 RCP suction nozzle safe end. Table 3-4 summarizes the allowable stresses for all loading conditions for the 1998 Code year with 2000 Addenda [3], which is applicable to the SB-166 replacement nozzle and weld material.

Table 3-3: Section III Allowable Stresses for RCP Suction Nozzle Safe end, 1974 Code Year [2]

Condition(2)	Stress Category(1)	ASME Reference	Limit	RCP Suction Nozzle Safe end	
				S_m or S_y (ksi)	Allowable (ksi)
Design	Primary Membrane Stress Intensity, P_m	NB-3221.1	S_m	17.0	17.0
	Local Primary Membrane Stress Intensity, P_L	NB-3221.2	$1.5S_m$	17.0	25.5
	Primary Membrane + Bending Stress Intensity ($P_L + P_b$)	NB-3221.3	$1.5S_m$	17.0	25.5
	Maximum Average Primary Shear Stress	NA – Pure shear stresses are only evaluated for the weld.			
Normal and Upset (Levels A and B)(3)	Primary + Secondary Stress Range ($P_m + P_b + Q$)	NB-3222.2	$3S_m$	17.0	51.0
	Cumulative Usage Factor	NB-3222.4	1	--	Ui < 1.0
	Maximum Average Primary Shear Stress	NA – Pure shear stresses are only evaluated for the weld.			
Test	Primary Membrane Stress Intensity, P_m	NB-3226(a)	$0.9S_y$	S_y = 30.0 ksi at 400°F	27.0
	Primary Membrane + Bending Stress Intensity ($P_L + P_b$)	NB-3226(b)	$1.35S_y$		40.5
Faulted (Level D)	Primary Membrane Stress Intensity, P_m	F-1323.1(b)	$2.4S_m$	17.0	40.8
	Primary Membrane + Bending Stress Intensity ($P_L + P_b$)	F-1323.1(b)	$1.5x2.4S_m$	17.0	61.2

Notes:

(1) ANSYS membrane stresses include general (P_m) and local (P_L) effects. The P_L evaluation is bounded by the P_m evaluation, which has lower allowable stresses.

(2) There are no emergency conditions specified for this design [22]. The plant leak test is included in the fatigue evaluation.

(3) The normal allowable stress for primary + secondary stresses is used to qualify the normal and upset transient cases. This is conservative because the allowable stresses may be increased by 10% for upset conditions.

Table 3-4: Section III Allowable Stresses for Replacement Nozzle and Weld, 1998 Code Year [3]

Condition[2]	Stress Category[1]	ASME Reference	Limit	SB-166 Alloy 690	
				S_m, S_y, or S_u (ksi)	Allowable (ksi)
Design	Primary Membrane Stress Intensity, P_m	NB-3221.1	S_m	23.3	23.3
	Local Primary Membrane Stress Intensity, P_L	NB-3221.2	$1.5S_m$	See Note 1	
	Primary Membrane + Bending Stress Intensity ($P_L + P_b$)	NB-3221.3	$1.5S_m$	23.3	35.0
	Maximum Average Primary Shear Stress (Minimum Allowable of Average and Maximum Shear Paragraphs)	NB-3227.2(a)	$0.6S_m$	23.3	14.0
		NB-3227.2(b)	$0.8S_m$		
Normal and Upset (Levels A and B)[3]	Primary + Secondary Stress Range ($P_m + P_b + Q$)	NB-3222.2	$3S_m$	23.3	69.9
	Cumulative Usage Factor	NB-3222.4	1	--	Ui < 1.0
	Maximum Average Primary Shear Stress (Minimum Allowable of Average and Maximum Shear Paragraphs)	NB-3227.2(a)	$0.6S_m$	23.3	14.0
		NB-3227.2(b)	$0.8S_m$		
Test	Primary Membrane Stress Intensity, P_m	NB-3226(b)	$0.9S_y$	S_y = 28.6 ksi at 400°F	25.7
	Primary Membrane + Bending Stress Intensity ($P_L + P_b$)	NB-3226(c)	$1.35S_y$[4]		38.6
	Maximum Average Primary Shear Stress (Minimum Allowable of Average and Maximum Shear Paragraphs)	NB-3227.2(a)	$0.6S_m$	23.3	14.0
		NB-3227.2(b)	$0.8S_m$		
Faulted (Level D)	Primary Membrane Stress Intensity, P_m	F-1331.1(a)	Lesser of $2.4S_m$, $0.7S_u$	S_m=23.3 S_u=80.0	55.9
	Primary Membrane + Bending Stress Intensity ($P_L + P_b$)	F-1331.1(c)	1.5 x P_m allowable	--	83.9
	Maximum Average Primary Shear Stress	F-1331.1(d)	$0.42S_u$	80.0	33.6

Notes:

(1) ANSYS membrane stresses include general (P_m) and local (P_L) effects. The P_L evaluation is bounded by the P_m evaluation, which has lower allowable stresses.

(2) There are no emergency conditions specified for this design [22]. The plant leak test is included in the fatigue evaluation.

(3) The normal allowable stress for primary + secondary stresses is used to qualify the normal and upset transient cases. This is conservative because the allowable stresses may be increased by 10% for upset conditions.

(4) Per Section NB-3226(c) [3], the allowable stress for $P_m + P_b$ is 1.35 S_y only when P_m is less than 0.67 S_y. The results for the SB-166 material in Section 3.2.3 show the maximum P_m for test condition is 12.39 ksi, which is less than 0.67 S_y (19.16 ksi).

3.1.3 Design Fatigue Curves for Section III Analysis

The design fatigue curves used in the fatigue analysis of the RCP suction nozzle safe end and the replacement nozzle and weld are tabulated from the appropriate ASME references, as shown in Figure 3-3 and Figure 3-4.

For the RCP suction nozzle safe end, the applicable fatigue curve is reported in Figure I-9.1 in Subsection NA of the 1974 Code [2]. The plot in Figure I-9.1 shows two curves, for ultimate tensile strength less than 80 ksi or between 115 ksi and 130 ksi. The dashed curve for $S_u < 80$ ksi is used for the SA-508 material. Figure 3-3 summarizes the data tabulated from Figure I-9.1. The alternating stress values are scaled based on the ratio of the modulus of SA-508 Class 1 at the maximum cycle temperature versus the modulus that the fatigue curve was developed for. In this case the modulus at temperature is taken at the design temperature of 650°F as 26.05×10^6 psi. The fatigue curve was developed for a modulus of 30.0×10^6 psi. The ratio is then calculated as 26.05/30.0.

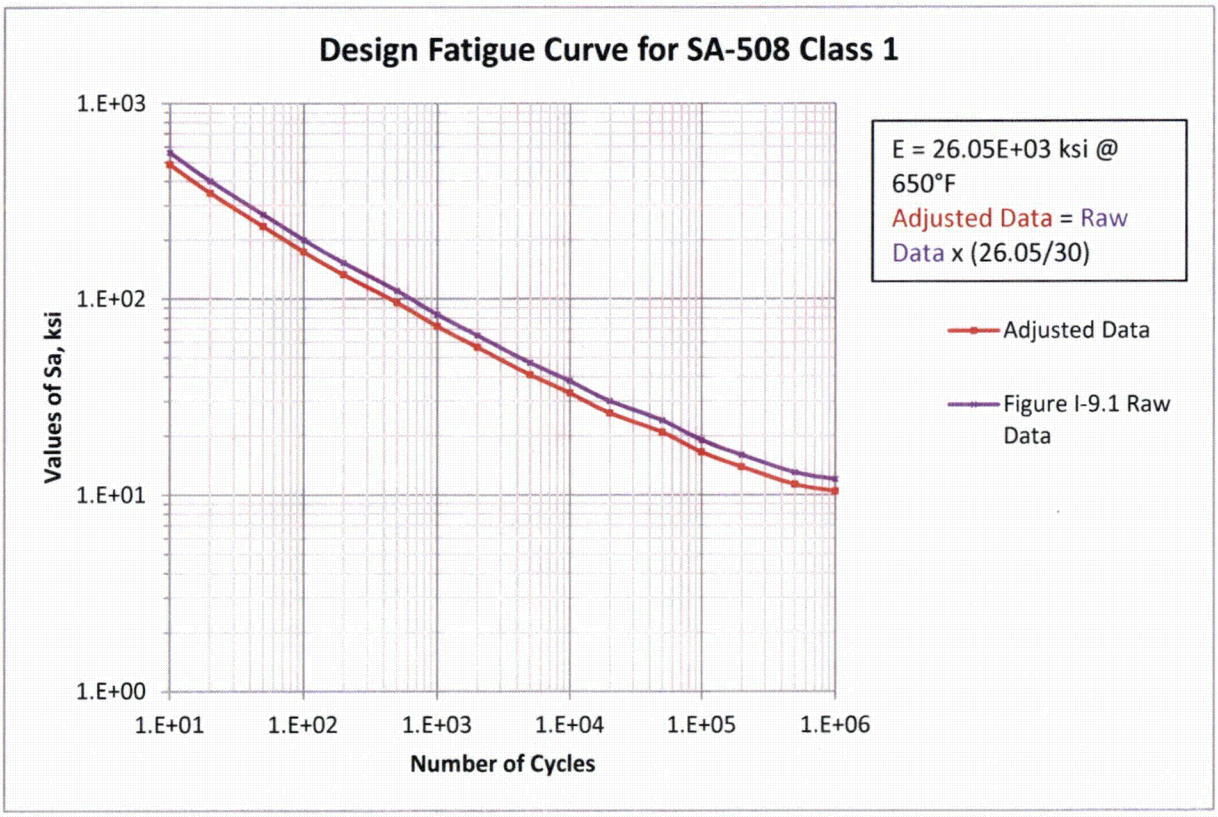

Figure 3-3: Design Fatigue Curve for SA-508 Class 1, per Figure I-9.1 [2]

The applicable fatigue curve for the replacement nozzle and weld SB-166 material is reported in Figure I-9.2.1 and Figure I-9.2.2 in Appendix I of the 1998 Code [3]. Figure 3-4 summarizes the data tabulated from the two figures (numerical values for the design fatigue curve are shown in Table I-9.1 and Table I-9.2.2 [3]). The data for curve C from Figure I-9.2.2 are used to obtain the most conservative result. The alternating stress values are scaled based on ratio of the modulus of SB-166 at the maximum cycle temperature versus the modulus that the fatigue curve was developed for. In this case the modulus at temperature is taken at the design temperature of 650°F as 27.85×10^6 psi. The fatigue curve was developed for a modulus of 28.3×10^6 psi. The ratio is then calculated as 27.85/28.3.

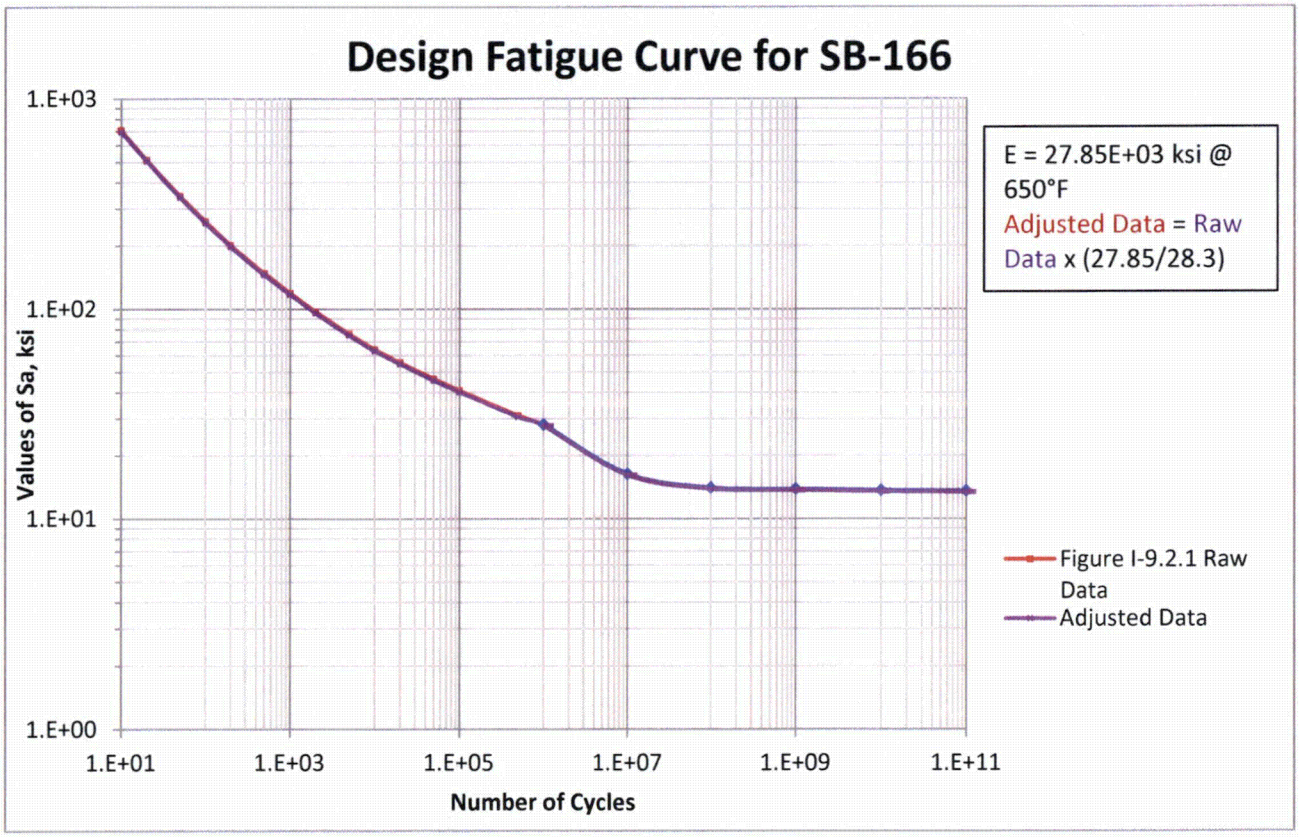

Figure 3-4: Design Fatigue Curve for SB-166, per Figure I-9.2.1 and Figure I-9.2.2 [3]

3.2 STRESS RESULTS

The stress results are separated into the following conditions: design, normal and upset (Levels A and B), test, and faulted (Level D). To evaluate the various stresses for each case, a set of 80 path locations was established to output linearized stresses at key locations. The same path locations were used for all cases. The result tables in this section show the worst-case path for each stress result. Plots showing these specific paths are included in Appendix A.

3.2.1 Design Condition

Table 3-5 summarizes the results for the design condition. All stresses are shown to be within the allowable limits of [2 and 3].

a,c,e

Table 3-5: Design Condition Stress Results

3.2.2 Normal and Upset Conditions (Levels A and B)

Table 3-6 summarizes the results for the normal and upset conditions. All stresses are shown to be within the allowable limits of [2 and 3]. The primary stress checks for Levels A and B conditions are bounded by the design condition evaluations. The Upset condition includes OBE loading, as well as an envelope transient including Reactor Trip, Loss of Flow, and Loss of Load. This enveloping transient goes slightly above design pressure. However, this increase in pressure is bounded by the 10% increase in allowable stresses for Level B conditions per NB-3223 [2 and 3].

The case pairings listed in Table 3-6 are for the highest stress range on each component.

a,c,e

Table 3-6: Normal and Upset Condition Stress Results

3.2.3 Test Conditions

Table 3-7 summarizes the results for the test condition. All stresses are shown to be within the allowable limits of [2 and 3].

a,c,e

Table 3-7: Test Condition Stress Results

3.2.4 Faulted Condition (Level D)

Table 3-8 summarizes the results for the faulted conditions. All stresses are shown to be within the allowable limits of [2 and 3].

Table 3-8: Faulted Condition Stress Results a,c,e

3.2.5 Fatigue Evaluation

Table 3-9 summarizes the results of the fatigue evaluation for the RCP suction nozzle safe end and the replacement nozzle. The total cumulative usage was calculated at each path node for the SA-508 suction nozzle safe end, SB-166 replacement nozzle, and replacement weld materials separately. The results of the fatigue evaluation include all Level A, Level B, and the leak test transient cases, including OBE loading.

Table 3-9: Fatigue Evaluation Results a,c,e

[ ]

3.3 VIBRATION ASSESSMENT

Section 4.3 of [23] states that the RCS may experience vibratory excitation with frequencies of:

- [ ]a,c,e CPS – lower range
- [ ]a,c,e CPS – middle range
- [ ]a,c,e CPS – upper range

The replacement instrumentation nozzle has relocated the attachment weld; therefore, the natural frequency of the nozzle and the attached Class 2 piping are evaluated to ensure that neither is within the excitation ranges.

This minimum piping frequency is [ ]a,c,e Hz and the instrumentation nozzle frequency is [ ]a,c,e Hz to [ ]a,c,e Hz. Both of these modes are outside of the restricted ranges, which is acceptable to avoid a resonant vibration issue. All other frequencies are well outside of the restricted ranges.

Since the replacement instrumentation nozzle was installed, APS has performed vibration testing to monitor the potential vibration of the system due to the repair. The evaluation in [24] shows that the maximum displacement of the system was no greater than [ ]a,c,e mils (peak-to-peak). The calculated peak velocity due to this level of vibration was [ ]a,c,e inches per second, which is well below the allowable of 0.5 inches per second [25], as discussed in [24].

4 FRACTURE MECHANICS EVALUATION

The fracture mechanics evaluation conservatively assumes that the entire radial extent of the partial penetration weld is hypothetically flawed in either the axial or circumferential orientation. Therefore, to support continued operation of Palo Verde Unit 3 with a half-nozzle repair to the RCP suction safe end instrumentation nozzle, a fracture mechanics evaluation is performed herein in accordance with the ASME Section XI acceptance criteria [1]. This evaluation demonstrates structural integrity of the RCP suction nozzle safe end with the flawed partial penetration weld for 40 years of plant operation. An operation duration of 40 years envelops the remaining life of Palo Verde Unit 3, including license renewal.

The evaluation performed herein also considers the analysis of small diameter Alloy 600/690 half-nozzle repairs in WCAP-15973-P-A [5] and Relief Request 31, which was previously submitted and approved for the Palo Verde Units 1, 2, and 3 small-bore hot leg Alloy 600 nozzles [6, 7, 30, 31].

The methodology used in the fracture mechanics evaluation is described in Section 4.1, which includes fatigue crack growth of the postulated flaw into the safe end base metal. Section 4.1 also discusses the structural integrity of the safe end base metal with the final flaw size after 40 years of fatigue crack growth. The crack growth and structural integrity results are provided in Section 4.2.

4.1 METHODOLOGY

In order to demonstrate structural integrity of the RCP suction nozzle safe end with the flawed partial penetration weld for 40 years of plant operation, a crack growth evaluation is first performed for a hypothetical initial flaw encompassing the entire radial extent of the abandoned partial penetration weld. Since the actual flaw size in the weld is not available, the initial flaw size is conservatively assumed to be the entire radial extent of the partial penetration weld, which would expose the RCP suction safe end base metal to the reactor coolant environment. The purpose of the fatigue crack growth (FCG) evaluation is to determine the growth of postulated axial and circumferentially oriented flaws, which are initially the size of the partial penetration weld, into the safe end base metal for a service life of 40 years. The primary growth mechanism in ferritic steels is due to fatigue crack growth, and the FCG rate for ferritic steel material in a pressurized water environment is based on the guidelines provided in Article A-4000 of the ASME Section XI Code [1]. The FCG evaluation is fully discussed in Section 4.1.1. The final flaw size after 40 years of fatigue crack growth is then evaluated based on the flaw size acceptance criteria of ASME Section XI, Appendix C, which is specific to the evaluation of flaws in piping.

According to ASME Section III, NA-3254.1, the boundary between the component (pump) and piping is the limit of reinforcement not closer than the first circumferential weld joint in welded connections. Therefore, for the purpose of the fracture mechanics evaluation contained herein, the RCP suction safe end is considered as part of the piping in accordance with ASME Section III, NA-3254.1. Therefore, the final flaw size after 40 years of fatigue crack growth is evaluated for acceptability based on the flaw size acceptance criteria of ASME Section XI, Appendix C, which is specific to the evaluation of flaws in piping.

The procedures of Article C-4220 of the ASME Section XI Code will be followed to determine the failure mode and analysis method. The screening criteria of Section XI Article C-4310 and Figure C-4220-1

provide the methodology for defining the appropriate analysis method of limit load, Elastic Plastic Fracture Mechanics (EPFM), or Linear Elastic Fracture Mechanics (LEFM).

The calculation of the flaw growth and the acceptability of the final flaw size are based on normal, upset, emergency, faulted and test conditions based on the pressure and thermal transient stresses and welding residual stresses in accordance with the 2001 Edition with 2003 Addenda of the ASME Code [1], which is the current code of record for Palo Verde Unit 3.

4.1.1 Fatigue Crack Growth

The fatigue crack growth analysis procedure involves postulating an initial flaw at the region of concern and predicting the growth of that flaw due to an imposed series of loading transients. The input required for a fatigue crack growth analysis is essentially the information necessary to calculate the range of crack tip stress intensity factors, ΔK_I, which depends on the crack size and shape, geometry of the structural component where the crack is postulated, and the applied cyclic stresses.

The normal, test, and upset operating transients from Table 2-1 are considered in the fatigue crack growth analysis. The full amount of transient cycles shown in Table 2-1 is distributed equally over a plant life of 40 years. The crack growth rate curves used for the ferritic steel are taken directly from Article A-4000 in Appendix A of the ASME Section XI Code [1]. The crack growth rate (da/dN) is a function of the applied stress intensity factor range (ΔK_I) and the R ratio (K_{min}/K_{max}) for the transient. The general form for fatigue crack growth is as follows:

$$da/dN = C_0(\Delta K_I)^n \qquad \text{(in./cycle)}$$

Where:

$$\Delta K_I = K_{max} - K_{min}$$

$$R = K_{min}/K_{max} \qquad (K_{min} > 0)$$

$$R = 0 \qquad (K_{min} \leq 0)$$

$$C_0 = 0 \text{ for } \Delta K_I < \Delta K_{th}$$

$$\Delta K_{th} = 5.0(1\text{-}0.8R)$$

According to Article A-4000 of the ASME Section XI code, the limiting crack growth results based on using the *n* and C_0 values for FCG in air from A-4300(b)(1) or those for water from A-4300(b)(2) should be used. The FCG rates for both environments are discussed below.

Fatigue Crack Growth Rate for Air (ΔK_I values in ksi$\sqrt{in}$):

$$da/dN = 1.99 \times 10^{-10} (S)(\Delta K_I)^{3.07} \qquad \text{(in./cycle)}$$

Where: $S = 25.72\ (2.88\text{-}R)^{-3.07}$

Fatigue Crack Growth Rate for Water (ΔK_I values in ksi$\sqrt{in}$):

$$\Delta K_{knee} = 17.74 \qquad (0 \leq R \leq 0.25)$$

$$\Delta K_{knee} = 17.74[(3.75\ R+0.06)/(26.9\ R-5.725)]^{0.25} \quad (0.25 < R < 0.65)$$

$$\Delta K_{knee} = 12.04 \quad (0.65 \leq R \leq 1.0)$$

For low ΔK_I values ($\Delta K_I < \Delta K_{knee}$):

$$da/dN = 1.02 \times 10^{-12}\ (S)(\Delta K_I)^{5.95} \quad \text{(in./cycle)}$$

Where:

$$S = 1.0 \quad (0 \leq R \leq 0.25)$$
$$= 26.9\ R-5.725 \quad (0.25 < R < 0.65)$$
$$= 11.76 \quad (0.65 \leq R \leq 1.0)$$

For high ΔK_I values ($\Delta K_I > \Delta K_{knee}$):

$$da/dN = 1.01 \times 10^{-7}\ (S)(\Delta K_I)^{1.95}\ \text{in/cycle}$$

Where:

$$S = 1.0 \quad (0 \leq R \leq 0.25)$$
$$= 3.75\ R + 0.06 \quad (0.25 < R < 0.65)$$
$$= 2.5 \quad (0.65 \leq R \leq 1.0)$$

The calculation of the stress intensity factor K_{max}, K_{min} will be determined based on the discussion given in Section 4.1.3.

4.1.2 Structural Integrity of the RCP Suction Safe End

After the fatigue crack growth of the hypothetical flaws into the RCP suction safe end base metal has been calculated, the acceptability of the final flaw size is determined based on the flaw size acceptance criteria in Appendix C of the ASME Section XI Code [1]. The first step in establishing the acceptability of the final flaw size is to determine the failure mode for the operating transients.

4.1.2.1 Determination of Failure Mode

Article C-4220 of the ASME Section XI Code defines the procedure used in the determination of failure mode and the analysis method for ferritic piping. In accordance with Figure C-4220-1 in the ASME Section XI Code, the Appendix C screening computations are used to determine the failure analysis method based on limit load, EPFM, or LEFM methodologies. The screening criteria are particularly important when metal temperatures are below the upper shelf of the Charpy Energy curve. At temperatures above the upper shelf of the Charpy Energy curve, the evaluation would be based on EPFM since the fracture toughness can be described with elastic plastic parameters at these higher temperatures.

Figure C-4220-1 of the ASME Section XI Code demonstrates the flow chart used with the screening criteria to select the analysis criteria. According to the flow chart the selection of the appropriate analysis method is as follows:

$$SC = K'_r/S'_r$$

$SC < 0.2$	Limit Load
$0.2 \leq SC < 1.8$	EPFM
$SC \geq 1.8$	LEFM

Where:

SC	=	Screening Criteria, dimensionless
K'_r	=	Ratio of stress intensity factor to material toughness, dimensionless
S'_r	=	Ratio of applied stress to the stress at limit load, dimensionless

The K'_r or S'_r terms are determined as follows:

$$K'_r = \left[1000\, K_I^2/(E' J_{IC})\right]^{0.5}$$

$$E' = E/(1-v^2)$$

$$S'_r = \sigma_p/\sigma_f$$

Where:

K_I	=	Applied stress intensity factor
E	=	Young's modulus
v	=	Poisson's ratio
J_{IC}	=	Measure of toughness due to crack extension
σ_p	=	Primary stress
σ_f	=	Flow stress, average of yield and ultimate strengths

For the S'_r term of the screening criteria, only primary stress should be considered as this term represents limit load due to plastic collapse. Also, the screening criteria computations contained in Article C-4000 are specific to semi-elliptical axial and circumferential flaws in a pipe; however, for the case contained herein the postulated flaws are in the shape of double corner flaws at the edge of a hole, as shown in Section 4.1.3. Therefore, the flow stress is conservatively used in the calculation of S'_r since the use of flow stress, instead of stress at limit load, would result in the more conservative LEFM failure mode. It should be noted that in the screening criteria, the primary, secondary, and residual stresses are included in the calculation of the K_I term.

Additionally, yield strength values based on ASME Section XI Table C-8321-1 for circumferential flaws and Table C-8322-1 for axial flaws are used in the screening criteria calculations. Since there is insignificant data to generate a Charpy impact energy curve based on the available Certified Material Test Report (CMTR) data, the upper shelf temperature is conservatively estimated to be at 200°F, as recommended by Appendix C of the ASME Section XI Code. The screening criteria are used to determine the appropriate failure mode and analysis method for low temperature time steps in select transients (i.e., Heatup/Cooldown). Above 200°F, the analysis method is based on EPFM since the fracture toughness can be described with elastic plastic fracture mechanics parameters.

The calculation of J_{IC} for axial and circumferentially oriented flaws is in accordance with paragraph C-8320. For axial flaws the J_{Ic} value can be estimated based on fracture toughness (K_{Ic}) as follows:

$$J_{Ic} = 1000(K_{Ic})^2/E'$$

The K_{Ic} value is determined based on ASME Section XI, Appendix A-4200, which provides a lower bound approximation of fracture toughness for ferritic material. Similarly for a circumferential flaw, paragraph C-8321 states that the J_{Ic} value may be determined based on reasonable lower-bound fracture toughness data. Therefore, the J_{Ic} value for use with circumferential flaws is determined in the same way as the axial flaw J_{Ic} value. In the transition temperature region, the fracture toughness can be represented by the following equation:

$$K_{Ic} = 33.2 + 20.734 \exp[0.02\ (T\text{-}RT_{NDT})]$$

Where K_{Ic} is in ksi$\sqrt{in}$, T and RT_{NDT} are as follows:

T	=	crack tip temperature (°F)
RT_{NDT}	=	reference temperature for nil ductility transition (°F)

For the RCP suction safe end, the RT_{NDT} is 40°F according to the RCP suction safe end Certified Material Test Report.

The methodology used in the LEFM and EFPM are described in the two following sections.

4.1.2.2 Linear Elastic Fracture Mechanics

The evaluation procedure and acceptance criteria used to demonstrate structural integrity of ferritic pipe in the LEFM regime is contained in Appendix C, Article C-7000 of ASME Section XI Code [1]. The LEFM evaluation is particularly important at temperatures below the Charpy upper shelf since at temperatures above the upper shelf on the Charpy Energy curve, the fracture toughness can be described with elastic plastic fracture mechanics parameters. To determine whether a flaw is acceptable for continued service without repair, the acceptance criteria for normal, upset, emergency, faulted, and test conditions must be met. The acceptance criteria are based on the crack tip stress intensity factor, as follows:

$$K_I \leq \left(J_{Ic}E'/1000\right)^{0.5}$$

Which simplifies to $K_I \leq K_{Ic}$ since the K_{Ic} value determined based on ASME Section XI, Appendix A-4200 is used to calculate J_{Ic} as discussed in Section 4.1.2.1. The determination of K_I is as follows [1]:

$$K_I = SF_m K_{Im} + SF_b K_{Ib} + K_{Ir}$$

Where:

K_I	=	Applied stress intensity factor including safety factors (Section 4.1.3)
K_{Im}	=	Stress intensity factor due to membrane stress (primary and secondary)
K_{Ib}	=	Stress intensity factor due to bending stress (primary and secondary)
K_{Ir}	=	Stress intensity factor due to residual stress

SF_m = Safety factor for membrane stress based on Service Level
SF_b = Safety factor for bending stress based on Service Level

The safety factors are from ASME Section XI paragraph C-2621 for circumferential flaws and C-2622 for axial flaws and are shown in Table 4-1. Test conditions are evaluated as Service Level B in accordance with paragraph C-2620.

Table 4-1: ASME Section XI, Appendix C Safety Factors

	Circumferential Flaw		Axial Flaw
Service Level	**SF_m**	**SF_b**	**SF_m**
A	2.7	2.3	2.7
B	2.4	2.0	2.4
C	1.8	1.6	1.8
D	1.3	1.4	1.3

4.1.2.3 Elastic Plastic Fracture Mechanics

The evaluation procedure and acceptance criteria used to demonstrate structural integrity of ferritic pipe in the EPFM regime are contained in Appendix C, Article C-6000 of ASME Section XI Code [1]. Additionally, general EPFM evaluation procedures for ferritic components in Appendix K of ASME Section XI Code and Regulatory Guide 1.161 [8] are used. Although the original purpose of Appendix K was to evaluate reactor vessels with low upper shelf fracture toughness, the general approaches in paragraph K-4220 and K-4310 are equally applicable to any region where the fracture toughness can be described with elastic plastic parameters. Therefore, the general procedures of Appendix K accompanied by Appendix C safety factors applied to the transient stresses will be used for the evaluation of the RCP suction safe end. The safety factors in Appendix C are more conservative than those used in Appendix K and are specific to piping. The suction safe end of the RCP has a 100% power normal operating temperature of approximately [ ]^{a,c,e} °F for consideration with the various operating transients. Furthermore, the temperature value of [ ]^{a,c,e} °F is considered to be sufficiently high and above the assumed upper shelf temperature of 200°F, which would thus result in ductile behavior of the material. Therefore, the use of elastic plastic fracture mechanics method is appropriate for the majority of the operating condition transients at high temperatures (above 200°F).

For EPFM, the acceptance criteria are to be satisfied for each category of transients, namely, Service Load Level A (normal), Level B (upset and test), Level C (emergency) and Level D (faulted) conditions. There are two criteria that must be satisfied for ductile stability. The first criterion is that the crack driving force must be shown to be less than the material toughness as follows:

$$J_{applied} < J_{0.1}$$

Where $J_{applied}$ is the J-integral value calculated for the postulated flaw under the applicable Service Level condition and $J_{0.1}$ is the J-integral characteristic of the material resistance to ductile tearing at a crack extension of 0.1 inch.

The second criterion is that the flaw must also be stable under ductile crack growth as follows:

$$\frac{\partial J_{applied}}{\partial a} < \frac{dJ_{material}}{da}$$

$$\text{at} \quad J_{applied} = J_{material}$$

Where:

$J_{material}$ = J-integral resistance to ductile tearing for the material

$\frac{\partial J_{applied}}{\partial a}$ = Partial derivative of the applied J-integral with respect to flaw depth, a

$\frac{dJ_{material}}{da}$ = Slope of the J-R curve

Material Resistance J-R Curve

One of the most important pieces of information for fracture toughness for pressure vessel and piping materials is the J-R (or $J_{material}$) curve of the material. The "J-R" stands for material resistance to crack extension, as represented by the measured J-integral value versus crack extension. Simply put, the J-R curve to cracking resistance is as significant as the stress-strain curve to the load-carrying capacity and the ductility of a material. Both the J-R curve and stress-strain curves are properties of a material.

Methods are available in NUREG/CR-5729 [9] that can generate J-R curves from available data such as material chemistry, radiation exposure, temperature, and Charpy V-notch energy. The method provided in [9] summarizes a large collection of test data, and presents a multivariable model based on advanced pattern recognition technology. Separate analysis models and databases were developed for different material groups, including reactor pressure vessel (RPV) welds, RPV base metals, piping welds, piping base metals and a combined materials group. For the evaluation herein, $J_{material}$ curves based on piping base metals in NUREG/CR-5729 will be used since it is the most appropriate representation of the RCP suction safe end material.

The material resistance, $J_{material}$, is fitted into the following equation [8, 9]:

$$J_{material} = (MF)C1(\Delta a)^{C2} \exp[C3(\Delta a)^{C4}]$$

Where, C1, C2, C3, and C4 are fitting constants, and Δa is crack extension. For the piping base metal model, the constants C1, C2, C3, and C4 are calculated based on the a_i and d_i constants from Table 13 of [9], which are defined below:

$$\ln C1 = a_1 + a_2 \ln CVN + a_3 T + a_4 \ln B_n$$
$$C2 = d_1 + d_2 \ln C1 + d_3 \ln B_n$$
$$C3 = d_4 + d_5 \ln C1 + d_6 \ln B_n$$

$$C4 = d_7$$

Where,

T = Temperature (°F)
B_n = Sample thickness (inches), conservatively taken as 1.0" per Reg. Guide 1.161 [8]
CVN = Charpy impact energy (ft-lbs)

Neutron irradiation has been shown to produce embrittlement that reduces the toughness properties of the reactor vessel ferritic steel material. The irradiation levels are very low in the RCP region and therefore the fracture toughness will not be measurably affected.

It should be noted that Margin Factors from Reg. Guide 1.161 [8] are included in the $J_{material}$ curve as follows:

MF = 0.749 for Service Levels A, B and C
MF = 1.0 for Service Level D

Applied J-curve

For small scale yielding, $J_{applied}$ of a crack can be calculated by the Linear Elastic Fracture Mechanics method based on the crack tip stress intensity factor, K_I, calculated as per Section 4.1.3. However, a plastic zone correction must be performed to account for the plastic deformation at the crack tip similar to the approach in Regulatory Guide 1.161 [8]. The plastic deformation ahead of the crack front is then regarded as a failed zone and the crack size is, in effect, increased.

Residual stresses are not considered in the EFPM evaluation in accordance with the document EPRI NP-6045 [10], which is the technical basis for the evaluation of flaws in ferritic piping (ASME Section XI Appendix C). According to [10], the residual stress can be neglected since experimental results from pipe tests show no evidence of residual stress effects on maximum load carrying capacity. Furthermore, the technical basis in EPRI NP-6045, Section 2-2.1, states that the conservatism included in evaluation procedures adequately account for any residual stress influence in the ductile tearing mode, and the explicit residual stress effects need not be included in the EPFM analysis. Additionally the technical basis for ASME Code Case N-749, PVP2012-78190 [11], which provides EPFM evaluation methodology for ferritic steel components, also confirms that residual stress should not be considered in EPFM evaluations. PVP2012-78190 states that cleavage failure, such as that of LEFM, is not an applicable failure mode when operating at the upper shelf, where the use of residual stresses can be overly conservative.

Thus continuing with the evaluation procedures, the K_I-values can be converted to $J_{applied}$ by the following equation:

$$J_{applied} = \frac{K_{ep}^2}{E'}$$

Where K_{ep} is the plastic zone corrected K-value, and $E'=E/(1-\nu^2)$ for plane strain, E = Young's Modulus, and ν = Poisson's Ratio. K_{ep} is the elastically calculated K_I-value based on the plastic zone adjusted crack depth or size. The plastic zone size, r_p, is calculated by

$$r_p = \frac{1}{6\pi}\left(\frac{K_I}{S_y}\right)^2$$

Where, S_y is the yield strength of the material. It should also be noted that safety factors from C-2620 are included on the transient stresses used in the calculation of stress intensity factors per ASME Section XI, Appendix C. The calculation of stress intensity factors are discussed in Section 4.1.3.

4.1.2.4 Primary Stress Limit

In addition to satisfying the fracture criteria, the primary stress limit of the ASME Code Section III, paragraph NB-3000 must be satisfied. The effects of a local cross-section area reduction that is equivalent to the area of the postulated flaw in the RCP suction safe end attachment weld must be considered by increasing the membrane stresses to reflect the reduced cross section. Membrane stresses in a thinned area of base metal due to the crack can be treated as a local primary membrane stress with an increased allowable stress intensity. The typical sizing is performed on the basis of the primary membrane stress intensity being less than Sm; however since the reduction in thickness is local, the permissible stress intensity is increased by 50%. This procedure is in accordance to the sizing calculation performed for WCAP-15973-P-A [5].

4.1.3 Generation of Stress Intensity Factors

Since the size of the actual indication(s) in the attachment weld was not detected at the time of the repair, a hypothetical flaw that extends radially over the entire Alloy 82/182 partial penetration weld is conservatively assumed. Flaws are projected in the axially and circumferentially oriented directions. The stress intensity factor expression for two corner flaws emanating from the edge of a hole in a plate from Annex C.4.4 of [12] is used in determining the stress intensity factor for the postulated flaw in the Alloy 82/182 partial penetration weld. The stress intensity factor can be expressed in terms of the membrane and bending stress components as follows:

$$K_I = (M_m (\sigma_m + p_c) + M_b \sigma_b) (\pi a/Q)^{1/2}$$

Where:

σ_m	=	Remote Membrane Stress Component
σ_b	=	Remote Bending Stress Component
p_c	=	Crack face pressure
M_m	=	Boundary Correction Factor for remote membrane [12]
M_b	=	Boundary Correction Factor for remote bending [12]
Q	=	Shape Factor per [12]
a	=	Depth of the corner flaw (See Figure 4-1)

Use of this method requires that the stresses be resolved into membrane and bending stress components. Stresses are resolved into membrane and bending components by first fitting the stresses to a 4th order polynomial as shown in Annex C.2.2.3 of [12]. Reference [12] calls for the use of remote membrane and bending stresses for use with the stress intensity factor expression due to stress concentration acting around the hole. Only primary stresses are affected by the stress concentration of the hole, therefore

remote primary membrane and bending stresses are used from the appropriate remote paths for the axial and circumferential flaw evaluations. Thermal transient and residual stresses from the paths at the location of the flaw are utilized in the calculation of stress intensity factors.

The stress intensity factor expression in [12] is applicable for a range of flaw shapes, with the depth of the flaw defined as "a", and the width of the flaw defined as "c", as shown in Figure 4-1. The corner cracks reflected in the axial and circumferential orientations are demonstrated in Figure 4-2 and Figure 4-3, respectively. The attachment weld shapes were based on the weld geometry shown in the RCP drawings in [19c] and [19d]. The nearest structural discontinuity to the nozzle is the pump reinforcement and it is used to determine the "W" term in the stress intensity factor calculations. The RCP suction safe end instrumentation penetration diameter (2R) = [ ]^{a,c,e} inch according to [19d].

The use of a plate model is acceptable since the lengths of the assumed flaws are small compared to the circumference of the pipe. Similar stress intensity factor databases based on plate geometry were also used in the determination of stress intensity factors in WCAP-15973-P-A [5].

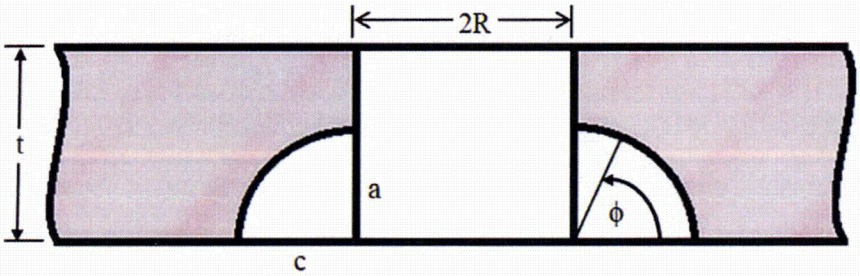

Figure 4-1: Corner Crack Geometry

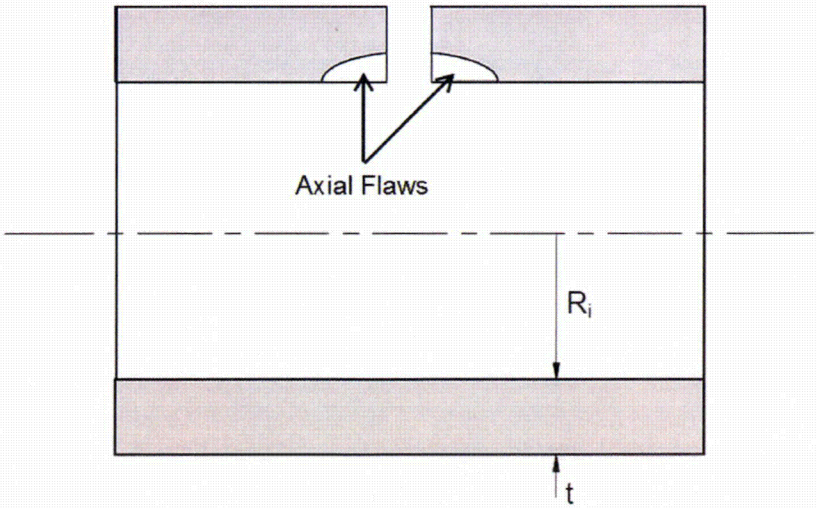

Figure 4-2: Axial Flaw Geometry

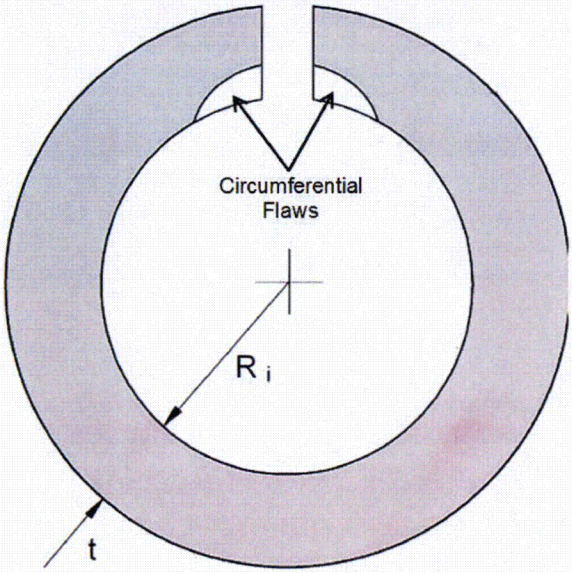

Figure 4-3: Circumferential Flaw Geometry

4.1.4 Transient Stress Analysis

In determining the acceptability of abandoning the flawed attachment weld in the RCP suction safe end, it is essential that all applicable loadings be considered. The first step of the evaluation is to determine the transient loading at the location of interest and, therefore, all the applicable pressure/thermal transients for the normal, upset, emergency, faulted, and test conditions must be considered. The applicable pressure/thermal transients and the corresponding transient cycles for the RCP suction safe end are discussed in Section 2.4. The corresponding design temperature and pressure transient curves are used in developing the time history through-wall pressure/thermal transient stress which is used as input to the fracture mechanics evaluation.

Transient stresses are determined based on the finite element analysis determined in Section 2, which modeled the area of interest in the RCP suction safe end. The model included the safe end base metal, Alloy 82/182 partial penetration weld, Alloy 600 instrumentation nozzle, Alloy 690 half-nozzle, 52M outside surface replacement weld, and the cladding. The safe end finite element model is shown in Figure 2-19. Stress contour plots of the limiting transients are provided in Section 2.7.

A total of 24 paths were used in the FEA model to extract transient stresses, which are shown in Figure 2-19. Paths 13 through 24 are reflections of Paths 1 through 12 across the instrumentation nozzle axis and will not be used since the resulting stress is similar to Paths 1 through 12. The paths used in the evaluation contained herein are Paths 1, 2, 5, 6, 7, 8, 11, and 12. Together Paths 1-2, 5-6, 7-8, and 11-12 are co-linear. Paths 1-2 and 7-8 are at the location of the welds and Paths 5-6 and 11-12 are remote from the welds. Paths 3-4 and 9-10 are not used since the stress intensity factors at these locations are not as limiting as those at Paths 1-2 and 7-8, respectively. It should be noted that evaluation results using Paths 3-4 and 9-10 were reviewed for thoroughness, and found to be not limiting. Hoop stress from Paths 1-2 and 5-6 are used for the axial flaw evaluation, and axial stress from Paths 7-8 and 11-12 are used for the circumferential flaw evaluation. Since the stress intensity factor definition from [12] calls for remote stresses to be used for mechanical loads, Paths 5-6 and 11-12 are used when calculating primary loading stress intensity factors. Paths 1-2 and 7-8 are used when calculating secondary loading (thermal transient) stress intensity factors.

All of the transients for normal, upset, faulted and test conditions are evaluated for the fracture mechanics evaluation as shown in Table 2-1. The Hydrostatic Test transient is also evaluated; however, since Palo Verde Unit 3 is already in operation, all hydrostatic tests must be in accordance with IWB-5000 of the Section XI ASME Code [1], which does not allow for hydrostatic tests of [ ]^{a,c,e} psia. Therefore, a maximum pressure of [ ]^{a,c,e} psia is used in the Hydrostatic Test transient. The Hydrostatic Test thermal transient stress is assumed to be the same as the Leak Test thermal transient stress since the temperature variation would be the same.

4.1.5 Welding Residual Stress Analysis

For the fracture mechanics evaluations, the initial postulated flaws were assumed to extend completely through the depth and width of the J-groove welds and through the nickel alloy buttering. The flaw geometry is thus conservatively considered as two corner cracks emanating from the edge of a hole in plate as shown in Figure 4-1.

Based on the welding residual stresses assessment provided in Section 3.2 of WCAP-15973-P-A [5], it was determined that for such a hypothetical large flaw configuration as described above, the residual stresses will not be present at the tip of the crack at the interface between the weld metal and carbon steel interface. During fabrication, the RCP safe end material was heat-treated after the buttering and prior to completion of the nozzle partial penetration weld; therefore, any welding residual stresses during the fabrication would be relieved at the butter to base metal interface. During the welding of the partial penetration weld, several layers of weld metal are typically deposited to develop the weld geometry of interest, each layer, after the initial layer of weld metal has the effect of reducing the residual stresses in the previous layers, thereby significantly reducing the residual stresses not only in the weld itself but also at the butter-base metal interface. Furthermore, any remaining high stressed locations in the buttering for the instrument nozzles will be removed by the grinding used to prepare the surface for dye penetrant inspection and for finishing the weld preparation, thus resulting in even lower stresses in the buttering.

Additionally, since residual stress is a displacement controlled load, the stresses resulting from the original welding process would decrease with the introduction of a hypothetical flaw completely through the J-groove weld. Also, any crack growth into the carbon steel suction nozzle safe end will further relieve the residual stresses.

However, for a conservative fracture mechanics evaluation, finite element welding residual stress analysis was performed in [13] using the Palo Verde Unit 3 specific RCP suction safe end configuration. The welding residual stress evaluation utilizes a 3-dimensional model of the safe end base metal, Alloy 82/182 partial penetration weld, Alloy 600 instrumentation nozzle, Alloy 690 half-nozzle, 52M outside surface replacement weld, and the cladding. The welding residual stress evaluation is performed by first modeling the welding of the instrumentation nozzle to the RCP suction safe end. Hydrostatic testing and normal operating conditions are then applied to the safe end before the half-nozzle repair is simulated in the model. The Alloy 82/182 partial penetration weld is simulated with a single weld pass of buttering followed by four equal volume weld passes. The 52M repair weld is simulated with three weld passes of roughly equal volume.

A total of twelve stress paths were used to present the residual stress data. Six paths each are on the axial and radial cross-sections as shown in Figure 4-4, each path is comprised of 21 points through the wall thickness. Paths 1, 2, 7, and 8 are utilized since these paths represent the local residual stresses at the deepest portion of the original weld. Paths 1 and 7 extend from the inside surface through the original attachment weld while paths 2 and 8 extend from the deepest extent of the original attachment weld, through the repair weld, to the outside surface. Together Paths 1-2 and 7-8 are co-linear. Paths 1-2 are used to obtain hoop welding residual stress for an axial flaw evaluation, and Paths 7-8 are used to obtain axial welding residual stresses for a circumferential flaw evaluation (see Figure 4-4). Stresses at Paths 3-4 and 9-10 were also investigated and found to be less limiting for the calculation of stress intensity

factors than Paths 1-2 and 7-8, respectively. The hoop and axial residual stress contour plots are shown in Figure 4-5 and Figure 4-6, respectively. The hoop and axial residual stress profiles at Paths 1-2 and 7-8 are shown in Figure 4-7 and Figure 4-8 respectively, and are denoted by the curve labeled "Analytical Residual Stress Profile [13]".

The analytical welding residual stresses are used in the fatigue crack growth and the structural integrity evaluation of the final flaw size for the LEFM calculations. However, based on engineering experience, the analytical welding residual stress evaluation are conservative as compared to actual welding residual stresses as discussed above in this section, particularly in the original Alloy 82/182 attachment weld. The welding residual stresses in the region of the original attachment weld are also beyond the yield strength of the material; therefore, it is appropriate to reduce the residual stresses to account for the plasticity of the material. Also as discussed above, the residual stress is a displacement controlled load, therefore, the residual stresses resulting from the original weld would decrease as a result of the postulation of a large initial flaw size and the subsequent flaw growth into the base metal. Therefore, in the LEFM analysis of select time steps at the beginning of heatup (time step = 1 second) and end of cooldown (time steps = 16664 seconds through 36000 seconds) where the fluid temperature is 70°F, the analytical welding residual stresses are reduced in the original attachment weld as shown in Figure 4-7 and Figure 4-8 to reduce over-conservatism. It is noted that the welding residual stresses are only reduced in the original Alloy 82/182 attachment weld, and the residual stresses through the remaining wall thickness are conservatively left unaffected. The reduced residual stress profile is used in only the LEFM fracture mechanics evaluation, and only at the select time steps mentioned above, to reduce conservatism in the welding residual stress profile through the original Alloy 82/182 attachment weld. The fatigue crack growth evaluation and all other time steps of the LEFM analysis are based on the full analytical residual stress profiles from Figure 4-7 and Figure 4-8.

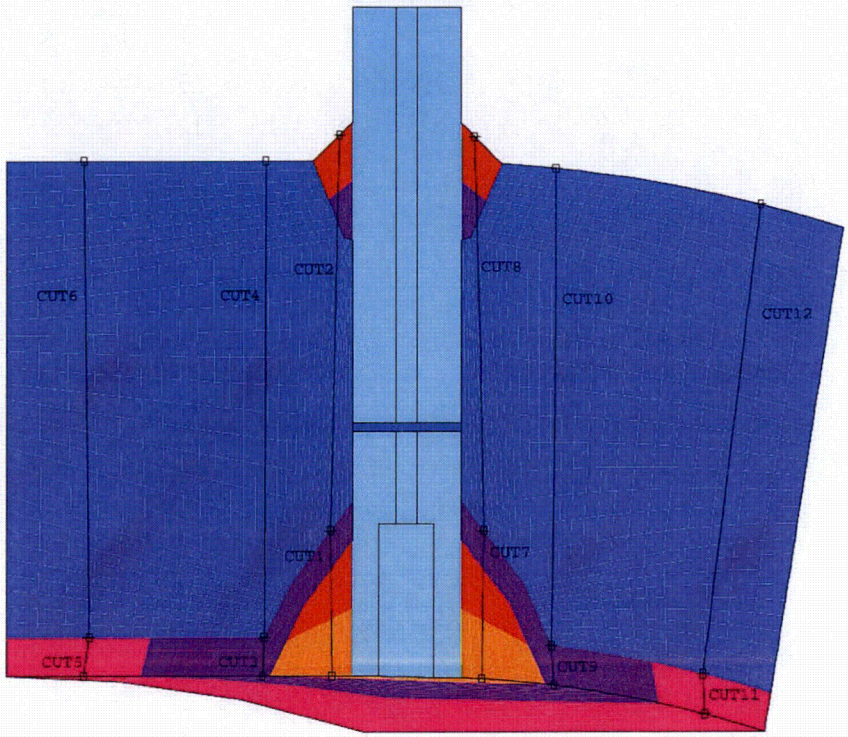

Figure 4-4: Residual Stress Evaluation Cut Paths [13]
(Viewed at 45° Angle to Axial Cut Plane)

a,c,e

Figure 4-5: Residual Hoop Stress Results (psi) [13]

a,c,e

Figure 4-6: Residual Axial Stress Results (psi) [13]

a,c,e

Figure 4-7: Through-Wall Welding Residual Hoop Stress Profile [13]

* Note that the residual stresses shown are through the entire wall thickness including the original attachment weld and the repair weld. Residual stresses beyond the original attachment weld are conservatively equal to the unreduced analytical residual stress profile [13].

a,c,e

Figure 4-8: Through-Wall Welding Residual Axial Stress Profile [13]

* Note that the residual stresses shown are through the entire wall thickness including the original attachment weld and the repair weld. Residual stresses beyond the original attachment weld are conservatively equal to the unreduced analytical residual stress profile [13].

4.2 FRACTURE MECHANICS EVALUATION RESULTS

A fracture mechanics evaluation is performed to demonstrate structural integrity of the RCP suction nozzle safe end with the flawed partial penetration weld for 40 years of plant operation. First a crack growth evaluation is performed for hypothetical initial flaws encompassing the entire radial extent of the abandoned partial penetration weld for growth into the RCP suction nozzle safe end due to the fatigue crack growth mechanism. Flaws are projected in the axially and circumferentially oriented directions for evaluation. The allowable flaw size criteria of Section XI, Appendix C of the ASME Code are then used to demonstrate that the final flaw sizes after 40 years of crack growth continue to meet the ASME Code margins. The results of the fatigue crack growth and structural integrity analysis are provided in Section 4.2.1 and 4.2.2 below based on the methodology discussed in Section 4.1.

4.2.1 Fatigue Crack Growth Evaluation

A fatigue crack growth analysis is performed according to the methodology in Section 4.1.1 to determine the final depth that the hypothetical postulated flaw in the RCP suction safe end instrumentation nozzle partial penetration weld would grow to after 40 years of operation. An operation duration of 40 years conservatively envelops the remaining operating life for Palo Verde Unit 3, including the License Renewal period.

Stress intensity factors based on a double corner cracked hole in a plate are first calculated for a range of flaw sizes based on primary, secondary, and residual stresses in the region of the attachment weld. Since there was leakage detected on the outside surface on the RCP suction safe end, the evaluation contained herein assumed that the initial flaw size radially encompasses the entire original attachment weld. Therefore, the initial postulated flaw will have a depth which extends through the Alloy 82/182 partial penetration weld to the base metal interface and a length equal to the width of the original weld prep. Flaws are projected in the axially and circumferentially oriented directions for evaluation and the respective stresses normal to the crack plane are used in the analysis. Crack growth is determined for this initial flaw due to the fatigue crack growth mechanism for a total of 40 years into the safe end base metal. The final flaw size with FCG will then be used to determine structural stability based on ASME Section XI, Appendix C.

In accordance with the stress intensity factors database for a double corner cracked hole in a plate, remote primary stresses are used in the calculation of the stress intensity factors to account for stress concentration around the penetration. Therefore, for the axial flaw projection, remote stresses at Paths 5-6 (Figure 2-19) of the transient stress model are used in the calculation of primary stress intensity factors. Similarly, for the circumferential flaw projection, remote stresses at Paths 11-12 (Figure 2-19) of the transient stress model are used in the calculation of primary stress intensity factors. Alternately, the stress intensity factor calculations for secondary and residual stresses utilized stresses at the location of the assumed flaw (Paths 1-2 for axial flaw and Paths 7-8 for circumferential flaw from Figure 2-19 and Figure 4-4).

The stress intensity factors used to calculate crack growth are determined at both the deepest point in the crack (Φ = 90°) and the surface point of the crack (Φ = 0°), and the limiting of the two are used to determine the final flaw size. In the FCG evaluation, the flaw depth to flaw width ratio is held constant

through the crack growth calculation. The complete design cycles from Table 2-1 are conservatively used in the FCG evaluation, even though the license renewal application demonstrates that the expected cycles for Palo Verde are projected to be less than the full count of the design cycles [14].

The crack growth results are shown in Table 4-2 for the axial and circumferential flaw configurations. The final flaw sizes after 40 years of operation are then used to determine the acceptability of continued operation of the Palo Verde Unit 3 RCP suction safe end as discussed in 4.2.2 below.

Table 4-2: Fatigue Crack Growth Results

Flaw Configuration	Initial Flaw Depth (in.)	Flaw Depth Including FCG			
		10 Years (in.)	20 Years (in.)	30 Years (in.)	40 Years (in.)
Axial Flaw	[				
Circumferential Flaw					]a,c,e

4.2.2 Final Flaw Stability Evaluation

4.2.2.1 Screening Criteria

Article C-4220 of the ASME Section XI Code defines the procedure used in the determination of failure mode and the analysis method. In accordance with Figure C-4220-1 in the ASME Section XI Code, the Appendix C screening computations are used to determine the appropriate ferritic piping analysis method using limit load, EPFM, or LEFM methodologies. The screening criteria (SC) are particularly important when metal temperatures are below the upper shelf of the Charpy Energy curve. Based on Article C-8000 of the ASME Section XI Code, in the absence of material specific data, an upper shelf temperature of 200°F shall be conservatively used. Therefore the screening criteria are used for all transients which experience transient temperatures below 200°F to determine the appropriate failure mode and analysis method. Once a transient experiences temperature above the upper shelf, the evaluation will be performed with respect to the EPFM methodology since the ferritic safe end would be at the upper shelf of the Charpy Energy curve and have sufficient ductility where structural stability can be determined based on EPFM.

The only Palo Verde Unit 3 transients that experience temperatures below 200°F are Heatup, Cooldown, Hydrostatic Test, and Leak Test. According to the piping design specification [23], at the beginning of the Heatup transient and at the end of the Cooldown transient, the temperature is [ ]a,c,e °F and the pressure is [ ]a,c,e psia. However, based on the Palo Verde Pressure-Temperature Limits in the Technical Requirements Manual [15], the maximum pressure at the beginning of Heatup or end of Cooldown is limited to [ ]a,c,e psia. Therefore, for the beginning of Heatup or end of Cooldown a maximum pressure of [ ]a,c,e psia is used in the screening evaluation.

For all instances of the Heatup, Cooldown, Hydrostatic Test, and Leak Test transients where the transient temperature is below 200°F, the ASME Section XI Article C-4000 screening criteria resulted in values greater than SC = 1.8 based on the calculations described in Section 4.1.2.1. Therefore, the more limiting

LEFM methodology will be used in determining the acceptability of the final flaw size for all instances of the Heatup, Cooldown, Hydrostatic Test, and Leak Test transients where the transient temperature is below the assumed Charpy upper shelf temperature (200°F). The screening criteria results for the most limiting time steps of each transient are shown in Table 4-3.

Table 4-3: Screening Criteria Results for Limiting Transient Time Steps

Transient	Limiting Time Step (sec.)	Axial Flaw SC	Circumferential Flaw SC
Heatup	3600	2.2	4.0
Cooldown	13680	2.2	3.4
Leak Test	61200	4.3	8.3
Hydrostatic Test	61200	4.0	7.6

4.2.2.2 Linear Elastic Fracture Mechanics

As discussed above, the LEFM methodology is used to evaluate transients that operate below the assumed Charpy upper shelf temperature of 200°F, which are notably Heatup, Cooldown, Hydrostatic Test, and Leak Test. The final flaw sizes after 40 years of FCG, as determined in Table 4-2, are then evaluated to determine acceptability based on the LEFM procedure of Section 4.1.2.2.

Stress intensity factors are determined using the primary and secondary transient stresses and welding residual stresses as discussed in Sections 4.1.4 and 4.1.5. The stress intensity factor database based on a double corner crack in a plate with a hole is used as discussed in Section 4.1.3.

Also as discussed above in Section 4.2.2.1, for the LEFM evaluation at the beginning of Heatup and at the end of Cooldown, a maximum pressure of [ ]^{a,c,e} psia is used in determining the stress intensity factor for the primary pressure loading.

The RCP design specification in [22] shows the Hydrostatic and Leak Test transient reaching a temperature as low as [ ]^{a,c,e} °F while the pressure is still elevated ([ ]^{a,c,e} psia for Hydrostatic and [ ]^{a,c,e} psia for Leak Test). According to the Palo Verde Pressure-Temperature Limits in the Technical Requirements Manual [15], the pressure of the Hydrostatic/Leak Test transient may not increase above [ ]^{a,c,e} psia unless the temperature is above [ ]^{a,c,e} °F. For the pressure in the Hydrostatic/Leak Test transients to be [ ]^{a,c,e} psia the temperature would have to be greater than [ ]^{a,c,e} °F. Therefore, for Hydrostatic and Leak Test transients, when the pressure is greater than [ ]^{a,c,e} psia, a temperature of [ ]^{a,c,e} °F is used in the LEFM evaluation.

For the evaluation of axial flaw, LEFM calculations were performed for a flaw depth of [ ]^{a,c,e} in., which is the predicted final flaw depth after 40 years of fatigue crack growth from Table 4-2. A LEFM fracture mechanics evaluation was performed for all Heatup, Cooldown, Hydrostatic Test, and Leak Test transient time steps with a temperature below 200°F and the most limiting results for each transient are shown in Table 4-4. The safety factors from paragraph C-2622 for axial flaws are included on the stress

intensity factors due to primary transient stress intensity factors per Appendix C-7000 of the ASME Section XI Code. There are no safety factors applied to the residual stress intensity factors according to Appendix C-7000 of the ASME Section XI Code.

For the circumferential flaw evaluation, LEFM calculations were performed for a flaw depth of [ ]^{a,c,e} in., which is the predicted final flaw depth after 40 years of fatigue crack growth from Table 4-2. A LEFM fracture mechanics evaluation was performed for all Heatup, Cooldown, Hydrostatic Test, and Leak Test transient time steps with a temperature below 200°F and the most limiting results for each transient are shown in Table 4-5. The safety factors from paragraph C-2621 for circumferential flaws are included on the stress intensity factors due to primary and secondary transient stress intensity factors per Appendix C-7000 of the ASME Section XI Code. There are no safety factors applied to the residual stress intensity factor according to Appendix C-7000 of the ASME Section XI Code.

The results in Table 4-4 and Table 4-5 are based on stress intensity factors from the deepest extent of the flaw. The results based on stress intensity factors at the deepest extent of the flaw were found to be more limiting than those at the surface point of the flaw. Based on the structural integrity results for axial and circumferential flaws in Table 4-4 and Table 4-5, the final flaw sizes after 40 years of crack growth are acceptable for continued operation based on the LEFM evaluation.

Table 4-4: LEFM Results for Axial Flaw
(Flaw Depth = [ ]a,c,e in.)

Transient	Time (sec.)	Temp (°F)	K_{Ip} (ksi√in)	K_{Is} (ksi√in)	K_{Ir} (ksi√in)	K_{Itotal} (ksi√in)	K_{Ic} (ksi√in)	K_{Itotal} / K_{Ic}
Heatup	1	[						
Cooldown	16664							
Leak Test	63000							
Hydro Test	63000							]a,c,e

Table 4-5: LEFM Results for Circumferential Flaw
(Flaw Depth = [ ]a,c,e in.)

Transient	Time (sec.)	Temp (°F)	K_{Ipm} (ksi√in)	K_{Ipb} (ksi√in)	K_{Ism} (ksi√in)	K_{Isb} (ksi√in)	K_{Ir} (ksi√in)	K_{Itotal} (ksi√in)	K_{Ic} (ksi√in)	K_{Itotal} / K_{Ic}
Heatup	1	[								
Cooldown	16664									
Leak Test	63000									
Hydro Test	63000									]a,c,e

4.2.2.3 Elastic Plastic Fracture Mechanics

Based on the Screening Criteria discussed in Section 4.2.2.1 all transients that operate above the Charpy upper shelf temperature of 200°F are evaluated using the EPFM methodology discussed in Section 4.1.2.3.

For the J-integral calculation, the key aspects of the analysis is to demonstrate that the magnitude of $J_{applied}$ is less than $J_{material}$ at 0.1 inch crack extension, and the slope of the $J_{material}$ curve is greater than the slope of the $J_{applied}$ curve at the intersection of the $J_{material}$ and $J_{applied}$ curves. In order to determine the $J_{applied}$ curve, the stress intensity factor, K_I, must be calculated based on the procedure shown in Section 4.1.3 for a double corner crack geometry for the applicable attachment weld geometry.

The most severe transients were evaluated since they will provide the highest combination of bending and membrane stresses from all transient time steps, which results in a limiting $J_{applied}$ curve. Additionally, the $J_{material}$ curves decrease at higher temperatures so transients with severe stress at higher temperatures would be limiting. Step Load Increase, Reactor Trip, and Loss of Secondary Pressure were selected since they were determined to result in the most limiting stress intensity factors for Normal, Upset, and Faulted conditions. It should be noted that all transients were considered in the EPFM evaluation.

In accordance with the stress intensity database from Section 4.1.3, remote membrane and bending stresses are used in the stress intensity factor calculations for primary stress to account for the influence of the stress discontinuity of the penetration hole near the stress cut. Secondary thermal transient stresses from path locations near the flaw are used in the stress intensity factor calculations. Residual stresses are not considered in the EFPM evaluation in accordance with the EPRI NP-6045 [10] and as discussed in Section 4.1.2.3.

Safety factors from Paragraphs C-2621 and C-2622 of the ASME Section XI Code, as shown in Table 4-1, are included in the stress intensity factors used in the EPFM evaluation. The safety factors are included in both the primary and secondary stress intensity factors used in the calculation of $J_{applied}$. The EPFM evaluation was performed for the deepest extent of the flaw since it was determined that the stress intensity factors at the deepest extent were more limiting than those at the surface point of the flaw.

The $J_{material}$ is determined based on the methodology in Section 4.1.2.3 from Reg. Guide 1.161 [8] and NUREG/CR-5729 [9]. For a conservative analysis, the CVN value used in the calculation of $J_{material}$ is the lowest of the six Charpy Impact tests from the CMTR at 100°F ([ ]^{a,c,e} ft.-lbs.). The RCP suction safe end CMTR does not provide sufficient data to generate the full Charpy Energy curve; therefore, it is conservatively assumed that the CVN values at a test temperature of 100°F represent the upper shelf even though the upper shelf temperature is not known and would be higher. The material resistance J-value, $J_{material,}$ is calculated using the maximum temperature from each transient. The higher temperature leads to a more limiting $J_{material}$ curve. The thickness of the safe end base metal is [ ]^{a,c,e} inches; however, a conservative value of B_n = 1.0 inch is used to be consistent with the Reg. Guide 1.161 [8]. Based on Reg. Guide 1.161, an MF = 0.749 is used for Levels A and B transients and an MF = 1.0 is used for Level D transients. Young's Modulus, E, and yield strength are from ASME Section III material properties for SA-508, Class 1 at the maximum transient temperature.

Once the $J_{applied}$ and $J_{material}$ are calculated, flaw stability is determined based on the J-R curves for the Palo Verde Unit 3 RCP suction safe end material as shown in Figure 4-9 through Figure 4-14 and Table 4-6. These results represent the most limiting transients for each service condition for both axial and circumferential flaw orientations. Based on the J-R curves, at a crack extension of 0.1 in., the $J_{material}$ curve is greater than the $J_{applied}$ curve for all transients. Additionally, at the point of intersection between the $J_{applied}$ curve and $J_{material}$ curve, the slope of the $J_{material}$ curve is greater than the slope of the $J_{applied}$ curve. Therefore, the final flaw sizes after 40 years of crack growth are acceptable for continued operation based on the EPFM evaluation.

Table 4-6: EPFM Results for Axial and Circumferential Flaws at 0.1" Crack Extension

Transient	Axial Flaw		Circumferential Flaw	
	$J_{applied}$ (kip-in/in^2)	$J_{material}$ (kip-in/in^2)	$J_{applied}$ (kip-in/in^2)	$J_{material}$ (kip-in/in^2)
Step Load Increase	[			
Reactor Trip				
Loss of Secondary Pressure				]a,c,e

a,c,e

Figure 4-9: EPFM Evaluation Results for Axial Flaw – Step Load Increase Transient (Normal Condition – Level A)

a,c,e

Figure 4-10: EPFM Evaluation Results for Axial Flaw - Reactor Trip Transient (Upset Condition – Level B)

a,c,e

Figure 4-11: EPFM Evaluation Results for Axial Flaw - Loss of Secondary Pressure Transient (Faulted Condition – Level D)

a,c,e

Figure 4-12: EPFM Evaluation Results for Circumferential Flaw - Step Load Increase Transient (Normal Condition – Level A)

a,c,e

Figure 4-13: EPFM Evaluation Results for Circumferential Flaw - Reactor Trip Transient (Upset Condition – Level B)

a,c,e

Figure 4-14: EPFM Evaluation Results for Circumferential Flaw - Loss of Secondary Pressure Transient (Faulted Condition – Level D)

4.2.2.4 Primary Stress Limit

The primary stress calculation is shown in Table 4-7 based on the calculation procedure in ASME Code Section III, paragraph NB-3000 [2]. The typical sizing is performed on the basis of the primary membrane stress intensity being less than S_m, however since the reduction in thickness is local the allowable stress intensity, S_m, is increased by 50%. This procedure is similar to the sizing calculation performed for WCAP-15973-P-A [5].

The largest flaw size after crack growth for either the axial or circumferential flaw is used in the primary stress limit evaluation to envelop all results. It should be noted that the final flaw depths shown in Table 4-2 include the cladding thickness which must be disregarded in the primary stress limit calculation. Therefore, the cladding thickness is subtracted from the flaw depth to represent the depth into the base metal only. As shown in Table 4-7 the limiting final flaw depth is acceptable with respect to the primary stress limit.

Table 4-7: Palo Verde Unit 3 RCP Suction Safe End Primary Stress Limit

Outside Radius (in.)	**Total Flaw Depth**(1) (in.)	**Flaw Depth into Base Metal**(2) (in.)	**Remaining Base Metal Thickness** (in.)	**Hoop Stress** (ksi)	**Radial Stress** (ksi)	**Stress Intensity** (ksi)	**1.5*Sm** (ksi)
[							]a,c,e

Notes:

(1) Final flaw depth from Table 4-2 for either axial or circumferential flaw.

(2) Thickness of base metal only, without cladding.

4.2.3 Corrosion

A general corrosion assessment of the nozzle bore diameter was performed in [16] for the half-nozzle repair one-cycle evaluation. The assessment in [16] determined the allowable increase in the diameter of the carbon steel safe end attachment nozzle bore due to corrosion of the pipe base metal would be at least [ ]^{a,c,e} inches. The allowable diametrical hole increase of [ ]^{a,c,e} inches was therefore compared to the corrosion growth of the bore hole calculated for 40 years.

The corrosion rate for a carbon steel material (such as that of SA-508, Class 1) for the Palo Verde Unit 3 RCP suction safe end is provided in [5]. The corrosion rate in [5], applicable to the half-nozzle crevice region, is provided for three separate operating conditions: full power operation, startup mode (assumed to be at intermediate temperature with aerated primary coolant), and refueling mode (100°F with aerated primary coolant). Arizona Public Service has committed to track the time at cold shutdown in the previous relief requests for hot leg Alloy 600 small-bore nozzle repairs in order to provide assurance that the allowable hole diameter is not exceeded over the life of the plant [16].

An overall corrosion rate was then determined based on the corrosion rates of the individual operating modes and the percentage of time spent in each mode. The calculated corrosion rate for Palo Verde Unit 3 was determined to be 1.53 mils per year (mpy) [16]. For a conservative operation period of 40 years, the total corrosion of the nozzle bore would be:

Corrosion = (1.53 mpy)(40 years) = (0.00153 in/yr)(40 yrs)

= 0.0612 inches (radially, relative to penetration)

= 0.1224 inches (diametrically, relative to penetration)

Since the expected corrosion in 40 years is only 0.1224 inches diametrically, the diameter of the bore would remain acceptable for the next 40 years of operation.

4.3 FRACTURE MECHANICS SUMMARY AND CONCLUSIONS

A fracture mechanics evaluation is performed to provide the technical basis for continued operation of the Palo Verde Unit 3 RCP suction safe end with a flawed instrumentation nozzle attachment weld. Flaw growth and stability evaluations were performed based on ASME Section XI to determine the acceptability of performing a half-nozzle repair and abandoning the flawed attachment weld for 40 years of plant operation. Acceptability of a flaw can be determined by first determining the amount of growth the hypothetical flaw would experience for the remaining life of the plant (40 years) and then verifying that the final flaw size after 40 years meets the acceptance criteria of ASME Section XI, Appendix C for ferritic piping.

Since the flawed location has not been inspected, the initial flaw size is conservatively assumed to be the entire radial extent of the partial penetration weld, which would expose the RCP suction safe end base metal to the reactor coolant environment. Flaw growth of this initial flaw size is performed for the RCP suction nozzle safe end due to the fatigue crack growth mechanism. The purpose of the flaw growth evaluation is to determine the growth of hypothetical postulated axial and circumferentially oriented flaws into the safe end base metal for a service life of 40 years. The allowable flaw size criteria of Section XI, Appendix C of the ASME Code are then used to demonstrate that the growth of the flaw in the original partial penetration weld into the safe end base metal remains acceptable for the remaining life of the plant.

The flaw growth evaluation is performed in Section 4.2.1 for axially and circumferentially oriented postulated flaws encompassing the original attachment weld. Flaw stability calculations are performed in Section 4.2.2 and demonstrate that the final flaw size from the flaw growth evaluation is acceptable according to the standards of the ASME Code. Based on the evaluation in Section 4.2, the final flaw size after 40 years of fatigue crack growth meets the ASME Section XI, Appendix C acceptance criteria.

An additional evaluation is contained in Section 4.2.3 of this calculation note which determines the acceptable life of the repair weld considering corrosion to the safe end base material which would increase the diameter of the attachment nozzle bore. This evaluation determined that it would take longer than 40 years for the hole to reach an unacceptable size due to corrosion in the region.

Since Palo Verde Unit 3 has less than 40 years of operation remaining, it is therefore technically justifiable to continue operation for the remaining life of the plant with a flawed attachment weld present in the RCP suction safe end, since the acceptance criteria of ASME Section XI have been met.

5 LOOSE PARTS EVALUATION

Because the half-nozzle repair process involves leaving a small remnant of the nozzle inside the existing penetration, the possibility that fragments of the existing partial penetration weld could come loose inside the RCS through the current planned end of plant life, which is 60 years, is evaluated. It is postulated, based on NDE performed to describe the flaws, that the crack(s) on the nozzle and/or weld are part-through-wall in the axial direction with no evidence of circumferential cracks. This is consistent with the orientation previously observed by APS for this type of degradation mechanism (i.e., PWSCC) in instrument nozzles in the hot leg.

The remnant Alloy 600 instrument nozzle (approximately 1.5 inches in length) is recessed inside the safe end bore. It remains constrained by a relatively tight radial clearance between the bore and the nozzle. For the half-nozzle repair to create a loose part, it would require continued degradation at the remaining portion of the original Alloy 600 nozzle and at the nozzle-to-casting J-weld wetted surface. Embrittlement, corrosion and wastage, fatigue, and stress corrosion cracking were considered as potential material degradation mechanisms. Based on a review of these degradation mechanisms, only PWSCC was identified as a potential active mechanism for material degradation that could potentially give rise to the production of loose parts. However, based on the tortuous, tight array of cracking created by PWSCC, as well as the fact that any non-adhered sections of material would be constrained from release by the surrounding material, it has been determined that continuation of PWSCC processes in the remnant Alloy 600 nozzle and J-weld is unlikely to result in liberation of loose material from the remaining in-place nozzle structure.

However, although it has been concluded that it is very unlikely that a loose part will be released from the Alloy 600 nozzle and/or J-weld, this evaluation conservatively addresses the possibility that one or more fragments of the existing partial penetration weld separates from the nozzle and weld butter and becomes a loose part inside the RCS. Based on this assumption, a conservatively sized fragment of weld was assumed to weigh approximately 0.1 pounds and have dimensions no greater than the partial penetration weld thickness at its cross-section, and a length of one-quarter of the circumference around the instrument nozzle.

Therefore, the structural and functional impacts of the loose weld fragment(s) on affected systems, structures, and components (SSCs) were evaluated. Engineering judgments were applied and prior PVNGS loose parts evaluation results were taken into consideration. The evaluation considered that although the aforementioned fragment represents one possible form of the loose part, it is possible that smaller fragments of different sizes, shapes, and weights could be released, or created. Additional smaller fragments are possible, for example, if a weld fragment was to make contact with a high-velocity RCP impeller blade, or perhaps make high-speed contact with the core support barrel.

The evaluation concluded that the postulated loose parts will have no adverse impact on the RCS and connected SSCs through the current planned end of plant life. The evaluation addressed potential impacts to various SSCs where the loose parts might travel. This included the RCPs, the main coolant piping, the reactor vessel and its internals, the fuel, the pressurizer, steam generators, as well as other systems attached to the RCS, including the spent fuel pool. It was determined that all impacted SSCs would continue to be capable of satisfying their design functions.

6 SUMMARY AND CONCLUSION

The purpose of this report is to demonstrate the acceptability of the half-nozzle repair for the flawed RCP suction safe end instrument nozzle at Palo Verde Unit 3. A 3-D finite element model is used to evaluate ASME Section III stresses and generate transient stress inputs for the fracture mechanics evaluation. The finite element model conservatively accounts for potential corrosion of the replacement J-groove weld applied for the half-nozzle repair.

Transient stresses and welding residual stresses were calculated using finite element methods and the stresses were used in the fracture mechanics evaluation. The fracture mechanics evaluation is performed in accordance with ASME Section XI and concludes that it is technically justifiable for Palo Verde Unit 3 to continue operation for the remaining life of the plant with a flawed attachment weld present in the RCP suction safe end.

The loose parts evaluation concluded that the postulated loose parts will have no adverse impact on the RCS and connected SSCs through the current planned end of plant life. It was determined that all impacted SSCs would continue to be capable of satisfying their design functions.

In conclusion, the half-nozzle repair implemented on the RCP Suction nozzle pressure instrumentation nozzle at PVNGS Unit 3 is acceptable and meets all applicable ASME Section III and Section XI criteria for the remaining life of the plant.

7 REFERENCES

1. ASME Boiler and Pressure Vessel Code, Section XI, 2001 Edition with 2003 Addenda.
2. ASME Boiler and Pressure Vessel Code, Section III, 1974 Edition.
3. ASME Boiler and Pressure Vessel Code, Section II and Section III, 1998 Edition up to and Including 2000 Addenda.
4. ASME Boiler and Pressure Vessel Code, Section II, 2013 Edition.
5. Westinghouse Report, WCAP-15973-P-A, Rev. 0, "Low-Alloy Steel Component Corrosion Analysis Supporting Small-Diameter Alloy 600/690 Nozzle Repair/Replacement Programs," February 2005. (Westinghouse Proprietary Class 2)
6. APS Letter, "Palo Verde Nuclear Generating Station (PVNGS) Units 1, 2, 3, Docket No. STN 50-528/529/530, 10 CFR 50.55a(a)(3)(i) Alternative Repair Request for Reactor Coolant System Hot Leg Alloy 600 Small-Bore Nozzles (Relief Request 31, Revision 1)." August 16, 2005. (ML Accession No. ML052550368)
7. NRC Letter, "Palo Verde Nuclear Generating Station, Units 1, 2, and 3 – Relief Request No. 31, Revision 1, Re: Proposed Alternative Repair for Reactor Coolant System Hot-Leg Alloy 600 Small-Bore Nozzles (TAC Nos. MC9159, MC9160, and MC9161). (ML Accession No. ML062300333)
8. Regulatory Guide 1.161, "Evaluation of Reactor Pressure Vessel with Charpy Upper-Shelf Energy Less Than 50 ft-lb."
9. E. D. Eason, J. E. Wright, E. E. Nelson, "Multivariable Modeling of Pressure Vessel and Piping J-R Data," NUREG/CR-5729, MCS 910401, RF, R5, May 1991.
10. *Evaluation of Flaws in Ferritic Piping.* Electric Power Research Institute, Palo Alto, CA: October 1988. EPRI NP-6045.
11. Proceedings of the ASME 2012 Pressure Vessel & Piping Conference, PVP2012-78190, "Alternative Acceptance Criteria for Flaws in Ferritic Steel Components Operating in the Upper Shelf Temperature Range."
12. American Petroleum Institute, API 579-1/ASME FFS-1 (API 579 Second Edition), "Fitness-For-Service," June 2007.
13. Dominion Engineering, Inc. Calculation C-8006-00-01, Rev. 0, "Palo Verde Reactor Coolant Pump Instrumentation Nozzle Repair Welding Residual Stress Analysis."
14. License Renewal Application, Palo Verde Nuclear Generating Station Unit 1, Unit 2, and Unit 3, Facility Operating License Nos. NPF-41, NPF-51, and NPF-74, Supplement 1, April 10, 2009.
15. Palo Verde Units 1, 2, and 3 Technical Requirements Manual, Rev. 62, November, 2014.
16. Westinghouse Report, DAR-MRCDA-15-6, Rev. 1, "Palo Verde Unit 3 RCS Cold Leg Alloy 600 Small Bore Nozzle Repair," April 2015. (Westinghouse Proprietary Class 2).
17. Westinghouse Letter, LTR-ME-15-65, Rev. 0, "ASME Code Section XI Reconciliation for Arizona Public Service (APS), Palo Verde Nuclear Generating Station (PVNGS) Unit 3 Replacement Instrument Nozzle," September 21, 2015.

18. Westinghouse Letter, LTR-SST-10-58, Rev. 2, "ANSYS 12.1 Release Letter," October 2, 2012.

19. Drawings

    (a) CE-KSB Pump Co. Inc. Drawing, C-8000-101-2017, Rev. 02, "Wall Static Pressure Nozzle Suction."

    (b) CE-KSB Pump Co. Inc. Drawing, E-8111-101-2002, Rev. 00, "Pump Casing – A."

    (c) CE Avery Drawing, STD-009-0009, Rev. 02, "Coolant Pumps Weld Joint Identification and Fabrication Requirements."

    (d) CE Avery Drawing, 339-0054, Rev. 00, "Safe End Mach. of Pressure Tap Holes & Weld Prep. (Suction)."

    (e) Westinghouse Drawing, C-14473-220-002, Rev. 0, "Replacement Pressure Tap Nozzle."

    (f) Westinghouse Drawing, E-14473-220-001, Rev. 0, "Pump Casing – A Pressure Tap Nozzle Modification Assembly."

    (g) Combustion Engineering Drawing, E-65473-771-001, Rev. 00, "General Arrangement Arizona Public Service III Piping."

20. CE-KSB Pump Co. Inc. MDL, MDL 8111-101-202, Rev. 00, "Material and Drawing List for Pump Casing 'A'," June 22, 1983.

21. CE-KSB Pump Co. Inc. MDL, 8000-101-217, Rev. 02, "Material and Drawing List for Static Pressure Nozzle – Suction," August 9, 1982.

22. Combustion Engineering Specification, SYS80-PE-480, Rev. 02, "Specification for Standard Plant for Reactor Coolant Pumps," May 10, 1978.

23. Combustion Engineering Specification, 00000-PE-140, Rev. 04, "General Specification for Reactor Coolant Pipe and Fittings," May 25, 1977.

24. Palo Verde Nuclear Generating Station Engineering Evaluation, 4642529, May 1, 2015.

25. ASME Standard, ASME OM3-1982, "Requirements for Preoperational and Initial Start-up Vibration Testing of Nuclear Power Plant Piping Systems," September 30, 1982.

26. Westinghouse Design Specification, 14273-PE-140, Rev. 15, "Project Specification for Reactor Coolant Piping and Fittings for Arizona Nuclear Power Project," June 25, 2007.

27. PVNGS Engineering Calculation, 13-MC-RC-503, Rev. 9, "RCS - RCP Pressure Differential System," November 16, 2010.

28. Palo Verde Nuclear Generating Station Specification, 13-PN-0204, Rev. 21, "Fabrication and Installation of Nuclear Piping Systems for the Arizona Public Company Palo Verde Nuclear Generating Station Unit 1, 2 and 3," May 2, 2014.

29. American National Standard, ANSI B16.11 - 1973, "Forged Steel Fittings, Socket-Welding and Threaded," ASME, New York, NY, 1973.

30. NRC Letter, "Palo Verde Nuclear Generating Station, Unit 2 Relief Request No. 31 RE: Proposed Alternative Repair for Reactor Coolant System Hot Leg Alloy 600 Small-Bore Nozzles (TAC No. MC6500)," May 5, 2005. (ML Accession No. ML051290123)

31. APS Letter, "Palo Verde Nuclear Generating Station (PVNGS) Unit 2 Docket No. STN 50-529 10 CFR 50.55a(a)(3)(i) Alternative Repair Request for Reactor Coolant System Hot Leg Alloy 600 Small-Bore Nozzles (Relief Request 31)," March 25, 2005. (ML Accession No. ML050950358)

APPENDIX A: ASME STRESS PATH LOCATIONS

The figures in this appendix show the path locations for the maximum stresses reported in Section 3.2. Von Mises plots of limiting stresses for the normal and upset conditions are also included. Each figure in this appendix shows a sliced view of the model to show the path location or stress results of interest. The term "cut" is used in the figures to denote a stress evaluation path.

A.1 RCP SUCTION NOZZLE SAFE END LIMITING PATHS

a,c,e

Figure A-1: Path Location 6

a,c,e

Figure A-2: Path Location 1

Note: The view shown is a slice of the RCP safe end with the top half removed. Path 1 is a radial path from the inside surface of the safe end to the outside of the safe end along the length of the instrumentation nozzle. The first point in the path is coincident with the remnant nozzle weld. The end point is coincident with the replacement nozzle weld.

a,c,e

Figure A-3: von Mises Stresses - Cooldown Transient at Step 5, Time 16,664 Seconds
Note: Stress displayed in the above figure is in units of psi.

a,c,e

Figure A-4: von Mises Stresses - 10% Step Increase Transient at Step 4, Time 686 Seconds
Note: Stress displayed in the above figure is in units of psi.

A.2 REPLACEMENT NOZZLE LIMITING PATHS

a,c,e

Figure A-5: Path Location 61

a,c,e

Figure A-6: Path Locations 58 and 60

a,c,e

Figure A-7: von Mises Stresses - Cooldown Transient at Step 4, Time 10,800 Seconds

Note: Stress displayed in the above figure is in units of psi.

a,c,e

Figure A-8: von Mises Stresses - Upset Transient at Step 5, Time 62.89 Seconds

Note: Stress displayed in the above figure is in units of psi.

A.3 ATTACHMENT WELD LIMITING PATHS

a,c,e

Figure A-9: Path Location 26

a,c,e

Figure A-10: Path Location 31

a,c,e

Figure A-11: Path Location 39

a,c,e

Figure A-12: Path Location 27

a,c,e

Figure A-13: Path Location 19

a,c,e

Figure A-14: Path Location 35

a,c,e

Figure A-15: von Mises Stresses - Cooldown Transient at Step 5, Time 16,664 Seconds with Cutout at Path 39

Note: Stress displayed in the above figure is in units of psi.

a,c,e

Figure A-16: von Mises Stresses - 10% Step Increase Transient at Step 4, Time 686 Seconds with Cutout at Path 39

Note: Stress displayed in the above figure is in units of psi.